Polymorphism in silica studied in the local density and generalized-gradient approximations

1999 J. Phys.: Condens. Matter 11 3833

(http://iopscience.iop.org/0953-8984/11/19/306)

J. Phys.: Condens. Matter **11** (1999) 3833–3874. Printed in the UK PII: S0953-8984(99)01205-9

Polymorphism in silica studied in the local density and generalized-gradient approximations

Th Demuth†§, Y Jeanvoine‡, J Hafner†§ and J G Ángyán‡

† Institut für Theoretische Physik and Centre for Computational Materials Science, Technische Universität Wien, Wiedner Hauptstraße 8–10, A-1040 Wien, Austria

‡ Laboratoire de Chimie Théorique, Institut Nancéen de Chimie Moléculaire, CNRS UMR 7565, Université Henri Poincaré, BP 239, F-54506 Vandoeuvre-lès-Nancy Cédex, France

Received 22 January 1999, in final form 19 March 1999

Abstract. The crystal structures of a large number of silica polytypes (α- and β-quartz, α- and β-cristobalite, β-tridymite, keatite, coesite and stishovite) have been studied using density functional theory, both in the local density approximation and including generalized-gradient corrections to the exchange–correlation functional. All crystal structures have been optimized by minimizing the total energy with respect to all lattice parameters and to the atomic coordinates within the unit cell (up to 40 structural parameters in the case of coesite). The $\alpha \rightarrow \beta$ transitions in quartz and cristobalite have been studied in detail, including different variants proposed for the structure of β-cristobalite. The tetragonal ($I\bar{4}2d$) and simple cubic ($P2_13$) structures are found to be energetically almost degenerate near the equilibrium volume. On volume expansion both structures converge towards the idealized highly symmetric $Fd3m$ structure. A similar continuous transition from a more compact orthorhombic ($C222_1$) to a highly symmetric hexagonal ($P6_3/mmc$) variant is also proposed for β-tridymite. For coesite two monoclinic variants (with $C2/c$ and $P2_1/c$ space-group symmetries, respectively) have been examined and found to be energetically degenerate to within 1 meV per SiO_2 unit. It is shown that within the local density approximation (LDA) the equilibrium atomic volume of all polytypes is predicted with an accuracy better than one per cent. The LDA also leads to excellent structural predictions and to accurate values of the bulk modulus. Corrections in the framework of the generalized-gradient approximation (GGA) lead to substantially larger equilibrium volumes, although at fixed volume the LDA and GGA lead to identical crystal structures. The increased volume also leads to less accurate structural parameters. However, we find that gradient corrections are essential for achieving accurate structural energy differences between the tetrahedrally coordinated phases found at larger atomic volumes (all polytypes except stishovite) and the octahedrally coordinated high-pressure polymorphs (stishovite and post-stishovite phases).

1. Introduction

Since silica is a fundamental building block of many rock-forming minerals, the structures and physicochemical properties have been the subject of numerous investigations for decades [1,2]. In addition, SiO_2 is widely used in the ceramic and glass industries and has an enormous application potential in optical fibres, in microelectronics and in catalysis. On the other hand, silica is one of the most difficult materials to study. The origin of this difficulty is in the enormous structural complexity. Silica exists in many different crystalline forms: α- and β-quartz, α- and β-cristobalite, tridymite, keatite, coesite and stishovite [3–6]. Most of these structures are composed of corner-sharing tetrahedral SiO_4 units with a fourfold-coordinated silicon at the centre and twofold-coordinated oxygen atoms at the corners. The structures differ

§ Present address: Institut für Materialphysik, Universität Wien, A-1090 Wien, Austria.

0953-8984/99/193833+42$19.50

only in the connectivity of the basic tetrahedral units and hence show only minimal structural energy differences. This is what makes an accurate calculation of the phase equilibria between the different silica polymorphs such a very delicate problem.

The discovery of stishovite, a dense polymorph of SiO_2 with octahedrally coordinated silicon [7] has excited enormous interest in the possibility of the existence of further dense octahedral phases at high pressure. It has been shown that at a pressure of 50 GPa, stishovite undergoes a displacive phase transition to a $CaCl_2$ structure [8]. Very recently, experimental as well as theoretical evidence for a number of possible post-stishovite phases with $Pnc2$-type [9, 10], $I2/a$ [11] and a variety of further structures has been proposed. Thus it appears that the structural complexity of the octahedral phases is at least equivalent to that of the tetrahedral low-pressure phases.

During the past decade considerable progress has been achieved in the computational modelling of phase stability and phase transitions in silica. In principle, the goal of such studies is not only to predict the physical properties of a material with a given crystal structure, but also to determine the equilibrium structure at a fixed temperature and pressure, starting from a random distribution of the atoms. The computationally less demanding approach is based on the use of empirical, semiempirical or first-principles-based interatomic force fields [12] and allows one to analyse the structural and physical properties of the silica polymorphs. For example, Boisen and co-workers [13] used a combination of dynamical simulated annealing and quasi-Newton minimization techniques to search for the global and local minimum-energy structures of ensembles with up to eight SiO_2 formula units distributed randomly in an asymmetric unit cell. The interatomic potentials are based on the quantum-mechanical potential energy function calculated for the molecule $H_2Si_2O_7$. Following this strategy, 23 distinct minimum-energy structures could be determined. Some of these structures could be identified with one of the known silica polymorphs; others are different from all known structures but nevertheless very close to the total energy of the known modifications. However, it remains uncertain whether a force field extrapolated from molecular calculations is sufficiently accurate to allow a reliable prediction of such subtle energy differences. Furthermore, studies based on more or less empirical potentials fall short of elucidating the deeper reasons for the coexistence of so many energetically almost degenerate polytypes. On the other hand, *ab initio* quantum-mechanical calculations of the atomic and electronic structure based on density functional theory in the local density approximation (LDA) or Hartree–Fock theories are independent of any biasing *ad hoc* assumptions and should—at least in principle—provide both accuracy and insight at the required level.

However, the quantum-mechanical modelling of the silica polytypes is a computationally very demanding task. This is due not only to the subtlety of the energy differences to be calculated. Further difficulties arise from the complexity of some of the crystal structures involved (coesite for example has seven inequivalent atomic positions within the unit cell in the proposed $C2/c$ structure and even twelve inequivalent positions in the $P2_1/c$ structure. Hence a complete optimization of the structure requires a minimization of the total energy with respect to up to forty independent lattice and internal parameters), from the strength and non-locality of the pseudopotentials necessary to describe the oxygen ion with the required accuracy, and from the limitations of the local density approximation in predicting structural energy differences between structures with very different local environments of the ions.

A significant advance beyond standard electronic structure methods based on the straightforward diagonalization of the full Hamiltonian matrix has been initiated by Car and Parrinello [14]. The basic idea is that, especially with a plane-wave basis, the number of eigenvalues required for a calculation of the ground state is much lower than the dimension of the Hamiltonian matrix. The lowest eigenvalues and the corresponding eigenvectors can

be calculated very efficiently using iterative diagonalization techniques such as simulated annealing [14] or a preconditioned conjugate-gradient method [15–17]. Still, because of the orthogonalization operations involved, the computational effort scales cubically with the number of atoms in the limit of very large systems. This scaling is significantly improved upon by using diagonalization techniques based on the minimization of the norm of the residual vector to each eigenstate [17], so nowadays calculations can be made for very large systems without any loss of accuracy [18].

All first-row elements (e.g. oxygen) are difficult to handle within a conventional norm-conserving pseudopotential scheme. Due to the lack of corresponding core states for cancellation, the 2p valence orbitals of these elements are tightly bound and sharply peaked near the ionic core. A hard pseudopotential and correspondingly a very large plane-wave basis set is required to cope with such a situation. The ultrasoft pseudopotentials introduced by Vanderbilt [19] offer the advantage of requiring significantly fewer plane waves than norm-conserving pseudopotentials while still providing an impressive degree of accuracy and transferability, matching that of the results obtained with the best available all-electron methods (for detailed comparisons see, e.g., references [20–23]).

Finally, a comparison of the total energies of crystalline phases with significantly different local environments (such as the tetrahedrally coordinated low-pressure/high-temperature polymorphs of silica on one hand and the octahedrally coordinated stishovite and post-stishovite phases on the other hand) goes to the very limits of the local density approximation (LDA). To cope with certain deficits of the LDA ('overbinding', i.e. overestimation of the equilibrium density and binding energy), generalized-gradient corrections (GGC) to the LDA have been introduced [24]. Applications of the more refined forms of these corrections to isolated molecules have demonstrated a marked improvement of structural and energetic predictions over the LDA [25, 26]. For the description of crystalline phase stabilities, the situation is not so clear. For the covalently bonded elements from groups IV to VI of the Periodic Table it has been shown that while at constant volume the gradient corrections hardly affect the predicted equilibrium structure, significant differences in the equation of state also lead to important changes in the calculated structural enthalpy differences at constant pressure and in the calculated transition pressures [20, 28]. The recent work of Hamann [29] suggests that at least the phase transition from α-quartz to stishovite is similarly affected by non-local corrections to the LDA [29].

To date, *ab initio* local density functional calculations have been performed for a number of silica polytypes: α-quartz [29–32], β-quartz [32, 33], α-cristobalite [30, 32, 34], β-cristobalite [32, 33, 35] and stishovite [29–33, 36, 37]. Teter *et al* [33] investigated also some of the hypothetical structures identified by Boisen *et al* [13]. A number of different possible octahedrally coordinated post-stishovite phases have recently been studied by Teter *et al* [38]. In addition to the pressure-induced transitions between crystalline polymorphs, the amorphization of α-quartz under pressure has been studied [39]. With the exception of the work of Park *et al* [36] and Cohen [37] who used the linearized augmented plane-wave (LAPW) method, all calculations have been performed within the pseudopotential framework. All investigations except the work of Hamann [29] on the α-quartz $\rightarrow$ stishovite transition use the LDA.

Ab initio Hartree–Fock calculations have been performed for α-quartz [40–43], α-cristobalite [44, 45] and stishovite [44, 46]. However, most of these calculations fall short of a full structural optimization of the complex crystal lattices and of quantitative calculations of the structural energy differences.

Hamann's work [29] on the quartz $\rightarrow$ stishovite phase transition demonstrates that only the gradient corrections lead to a reasonably accurate prediction of the transition pressure.

The important result is that while the LDA calculations predict an energy difference of only 0.086 eV per SiO_2 unit (Keskar and Chelikowsky, reference [31]), 0.07 eV (Liu *et al*, reference [32], gradient corrections lead to a significant enhancement of the structural energy difference to $\Delta E = 0.57$ eV/SiO_2 unit (Hamann, reference [29]), in coincidence with the Hartree–Fock result of $\Delta E = 0.57$ eV/SiO_2 unit [46] and with the experimental estimate $\Delta E = 0.54$ eV/SiO_2 unit of Holm *et al* [47] and of Akaogi and Navrotsky [48]. As demonstrated by Hamann, this has a very strong influence on quantitative predictions of the α-quartz $\longrightarrow$ stishovite transitions.

The analysis of the available theoretical results suggests that the LDA predictions for the structural phase stability of the other quartz polymorphs have to be re-examined with a view to finding the possible influence of non-local corrections to the exchange–correlation functional. The problem is also complicated by the fact that although the GGA definitely improves the predicted structural energy difference, the gradient-corrected equilibrium density, bulk modulus and equation of state are not consistently better than the LDA predictions [29]. In addition, the more complex tetrahedral polymorphs of silica such as tridymite [49], keatite [50] and coesite [51] have not yet been examined using *ab initio* methods.

In the present work we report on local density functional and generalized-gradient calculations of the structural and cohesive properties of α- and β-quartz, α- and β-cristobalite, tridymite, keatite, coesite and stishovite. We believe that our work is of interest for several reasons. First, we investigate a larger range of silica polymorphs than are treated in any other previous study. It is also important that the uniform theoretical treatment facilitates systematic comparisons and the identification of trends. Second, we present the first *ab initio* investigation of the more complex polytypes. Third, we investigate the pressure-induced changes in the crystal structure in sufficient detail to allow us to develop a microscopic picture of the phase transitions.

2. Theory

For our calculations we used the Vienna *ab initio* simulation package (VASP) [16, 17], which is based on the following principles:

(a) We use LDF theory [52, 53] with the exchange–correlation functional given by Ceperley and Alder as parametrized by Perdew and Zunger [54]. Generalized-gradient corrections to the local exchange–correlation functional have been treated as proposed by Perdew *et al* [25]. Alternatively, the exchange functional of Perdew [55] together with the correlation functional proposed by Becke [26, 56] have been used to test the influence of different approximations to the gradient functional.

(b) The solution of the generalized Kohn–Sham equations is performed using an efficient matrix-diagonalization routine based on a sequential band-by-band residual minimization method (RMM) applied to the one-electron energies [17, 57].

(c) In the doubly iterative RMM method it is essential to use an efficient charge-density mixing routine to avoid charge-sloshing problems. We use an improved Pulay mixing for calculating the new charge density and potential [58]. We have found that the sequential band-by-band algorithm combined with an efficient mixing algorithm is considerably faster than conjugate-gradient (CG) algorithms attempting a direct minimization of the energy by treating all bands simultaneously [17].

(d) The optimization of the atomic geometry is performed via a conjugate-gradient minimization of the total energy with respect to the volume and shape of the unit cell and to the atomic coordinates. The structural optimization was terminated when the

energy difference between two successive steps became smaller than 10^{-5} eV. In addition, a requirement for convergence is that all forces acting on the atoms are smaller than 0.03 eV $Å^{-1}$.

(e) After moving the atoms, the new charge densities are estimated by extrapolating the results of the last few steps.

(f) The calculation has been performed using fully non-local optimized ultrasoft pseudopotentials [19, 20]. The non-local contributions are calculated in real space, using the optimized projectors introduced by King-Smith, Payne and Lin [59]. Details of the pseudopotentials are given in references [20, 21]. The cut-off energy for the plane-wave basis set was $E_{\mathrm{cut}} = 396$ eV; for the augmentation charges a cut-off of 829 eV was used.

(g) Brillouin-zone integrations were performed using a grid of Monkhorst–Pack special points [60] and using the linear tetrahedron method [61] with the corrections proposed by Blöchl *et al* [62]. This technique is most appropriate for semiconducting systems.

(h) The energies calculated as a function of volume were interpolated using a Murnaghan equation of state [63, 64]. This equation was used to estimate the pressure, the bulk modulus and its pressure derivative. Our choice between the Birch–Murnaghan and Murnaghan equations of state was motivated by the fact that the latter is valid over a wider range of pressures [64]. However, it was found that a reasonable quality of the fit could be achieved only if a rather fine-grained mesh of volumes was used, and even then the fit is good only over a restricted range of volumes. The reason for this is that the energy–volume curves (especially those of the low-temperature forms of quartz and cristobalite) are affected by the proximity of a structural phase transition.

3. Theory of silica polymorphs

Only very recently an attempt has been made to describe the structural relationships between the silica polymorphs within the framework of current theories of structural phase transitions. Dmitriev *et al* [65] proposed describing the crystal structures of the silica polymorphs as the results of ordering and displacive transformations from a parent disordered body-centred cubic structure with different fractional occupancies of SiO_2 units. The degree of occupancy varies from 1 in the high-pressure stishovite phase over 2/3 in the intermediate- and low-pressure phases of coesite and quartz to 1/2 in the low-pressure–high-temperature phases of tridymite and cristobalite. This structural relationship might ultimately lead to a microscopic scenario for the reconstructive transitions between these structures completing, together with the established descriptions of the displacive phase transitions between the high- and low-temperature forms of cristobalite and quartz [66, 67], our understanding of the polymorphism in silica. The aim of the present study is to give a complete account of the structure and energetics of the silica polymorphs on the basis of *ab initio* density functional theory and in addition to contribute to the understanding of the mechanism of the structural phase transitions.

3.1. Quartz

In the low- and high-temperature forms of quartz, SiO_4 tetrahedra are arranged on pairs of helical chains spiralling in the same sense around a hexagonal screw axis. According to the direction of the rotation, one distinguishes between left- and right-handed forms of 'high'- and 'low'-quartz. The structure of 'low'- (or α-) quartz may be considered as a distorted form of the idealized structure of 'high'- (or β-) quartz. The distortion may be described as a rigid rotation of the SiO_4 tetrahedra about the (100) axis (see figure 1). In the β-polymorph the tilt angle δ is zero; in the α-form one has $\delta = \pm 16.3^{\circ}$ (reference [71]). There is, however,

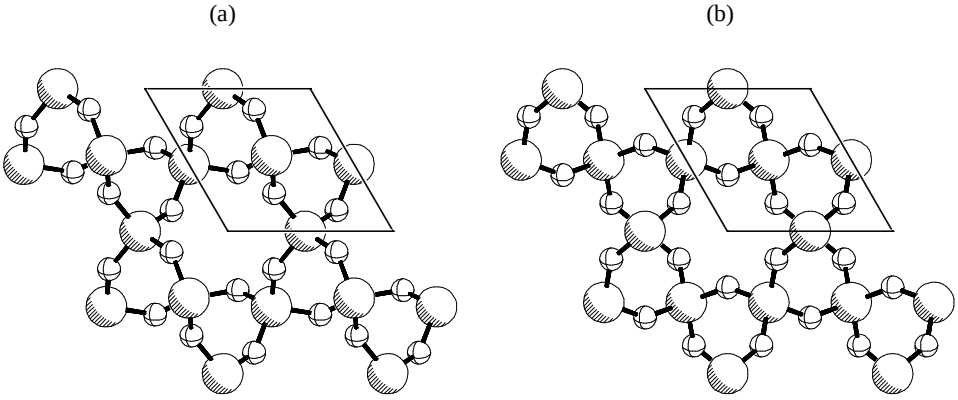

Figure 1. Representations of the α-quartz (a) ($P3_221$) and β-quartz (b) ($P6_222$) structures. Large spheres represent Si; small spheres represent O atoms.

still some controversy as regards whether in the β-phase the atoms really occupy the high-symmetry positions or whether the β-structure is no more than a disordered array of small domains of the α-form [67–69]. Hence there is a particular interest in studying the variations of the equilibrium structures on approaching the phase transition.

Table 1. Structural parameters, bond lengths (in Å) and bond angles (in degrees), cohesive energies and bulk moduli for α-quartz ($P3_221$). δ is the tilt angle of the SiO_4 tetrahedra relative to the symmetric orientation in α-quartz.

	Experiment[a]	GGA[b]	LDA[b]	GGA[c]	LDA[c]
a (Å)	4.9160	5.0271	4.8992	4.97	4.84
c (Å)	5.4054	5.5089	5.3832	5.52	5.41
c/a	1.1001	1.0958	1.0988	1.1107	1.1178
V/SiO_2 (Å^3)	37.71	40.19	37.30	39.36	36.58
Si(u)	0.4697	0.4814	0.4695		
O(x)	0.4135	0.4165	0.4143		
O(y)	0.2669	0.2460	0.2670		
O(z)	0.1191	0.1364	0.1199		
Si–O	1.6137	1.6170	1.6045	1.622	1.611
Si–O	1.6046	1.6137	1.5987	1.625	1.617
O–Si–O	109.0	108.4	109.3		
O–Si–O	110.5	110.4	110.4		
O–Si–O	108.8	109.5	108.8		
O–Si–O	109.2	108.8	109.2		
Si–O–Si	143.7	149.5	144.1	143.7	145.5
δ	−16.3	−10.4	−15.9		
E_0 (eV/SiO_2)		−23.8261	−25.9641		
B_0 (GPa)	34–37	31.3	35.4	48	45
B_0'	5.99	3.1	4.9	3.0	4.9

[a] Reference [102] for the structure data; references [102], [72] and [73] for the bulk moduli.
[b] Present work.
[c] Reference [29].

3.1.1. α-quartz. α-quartz has the hexagonal space-group symmetry $P3_221$ for the right-handed enantiomorph and $P3_121$ for the left-handed form. In addition, the tilt angle can be positive or negative, leading to four different forms of α-quartz. The different orientations of the tilt are related to the formation of Dauphiné twins. Natural α-quartz is a mixture of Dauphiné twins differing only in the sign of the tilt angle. The primitive unit cell contains three formula units. At a fixed volume, five parameters must be determined to specify the structure: the axial ratio c/a and the internal parameters u, x, y, z. Si atoms occupy the Wyckoff positions (3a) with coordinates $(u, 0, 2/3)$, O atoms the positions (6c) with coordinates $(x, y, \frac{2}{3} + z)$. Throughout this work we shall use the notation (u, v, w) for the internal parameters of silicon and (x, y, z) for oxygen. Table 1 presents the results of the structural optimizations performed in the local density and generalized-gradient approximations (Brillouin-zone integrations have been performed using a $3 \times 3 \times 3$ grid, corresponding to 14 irreducible $\vec{k}$-points) in comparison

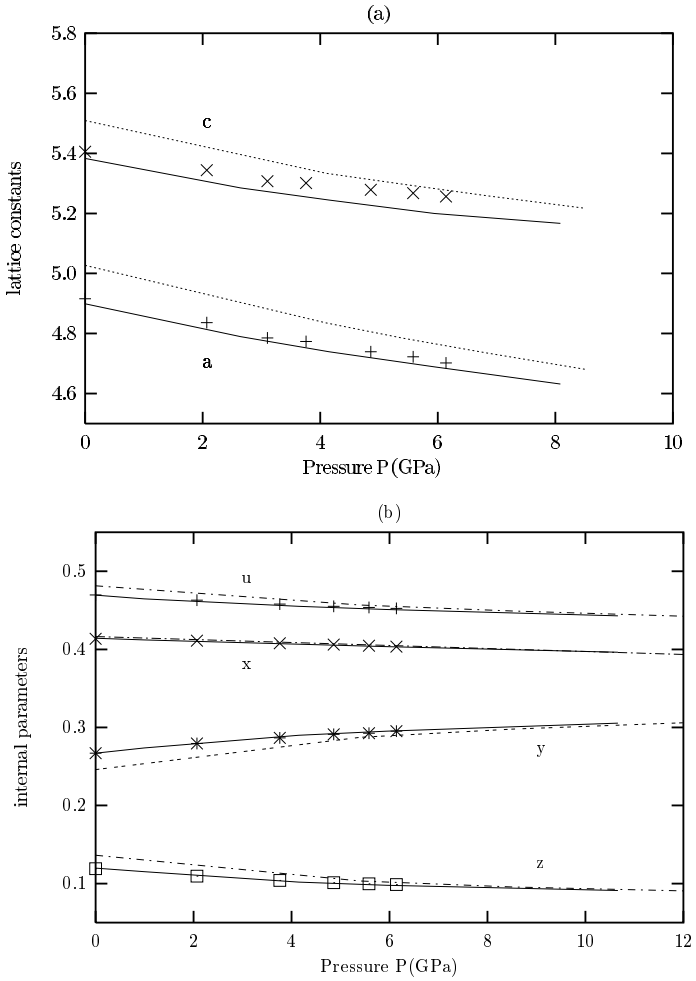

Figure 2. The calculated variations of the lattice constants a and c (part (a)) and of the internal structural parameters (b) u(Si), x, y, z(O) of α-quartz (cf. text) with pressure. Solid curves represent LDA results; broken curves represent GGA results. The points represent the experimental data of Levien *et al* given in reference [71].

with the experimental data. For the lattice constants we use the data obtained very recently by Angel *et al* [70], the internal parameters are from the structural refinement of Levien *et al* [71] and the values of the bulk moduli from references [71–74]. The first important thing to note is that the LDA predicts the equilibrium volume per SiO_2 unit with an accuracy of 1%, whereas the GGA leads to an overestimate of 6.6%. The LDA also leads to a consistently more accurate description of all internal parameters, of the distortion of the SiO_4 tetrahedra (note in particular the O–Si–O bond angles), of the tilt angle of the tetrahedra with respect to the high-symmetry orientations and of the bulk modulus. Equilibrium volumes determined in previous LDA [29, 31–33] calculations scatter between $V = 36.58$ Å^3 and $V = 38.55$ Å^3; all are less accurate in the prediction of the internal parameters. The GGA calculation of Hamann [29] predicts an increase of the volume with respect to the LDA value of ∼7.6%, in agreement with the present results.

The calculated variations of the internal parameters under pressure are compared in figure 2 with the experimental data of Levien *et al* [71]. We find a very good agreement of the LDA data with experiment, while there is a systematic deviation in the GGA results. However, this does not reflect a different description of the atomic arrangement, but merely a superposed isotropic pressure arising from the gradient corrections. The bulk modulus B_0, its pressure derivative B_0' and the equation of state (see figure 3) are consistently better described in the LDA approximation.

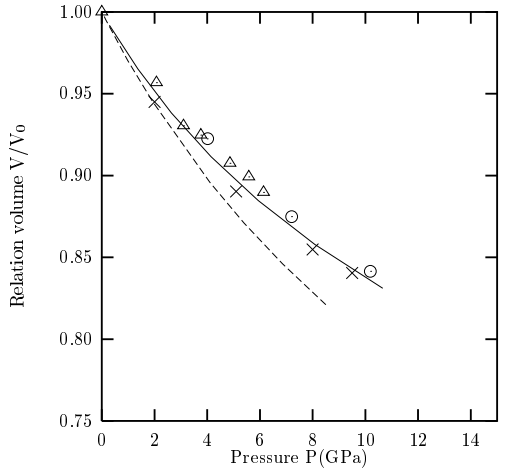

Figure 3. The equation of state of α-quartz, calculated in the LDA (solid curves) and GGA (broken curves). The points represent the experimental data of Hazen *et al* (reference [73], crosses), Glinnemann *et al* (reference [72], circles) and Levien *et al* (reference [71], triangles).

3.1.2. β-quartz. The idealized structure of 'high'- or β-quartz has space-group symmetry $P6_222$ for the right-handed form and $P6_422$ for the left-handed enantiomorph. The unit cell contains nine atoms; Si occupies the Wyckoff positions (3c) and O the positions (6j) with coordinates $(x, 2x, 1/2)$. Hence at fixed volume there are only two structural parameters to be determined. The $\vec{k}$-point sampling has been performed on the same $3 \times 3 \times 3$ grid of special points as for α-quartz, but due to the higher symmetry the number of irreducible points is reduced to six. Our results are compiled in table 2, compared with the experimental data of Wright and Lehmann [75] for the structure. Both the LDA and the GGA overestimate the equilibrium volume, the LDA by 2%, the GGA by 5.5%. Hence the influence of the gradient

Table 2. Structural parameters, bond lengths (in Å), bond angles (in degrees), cohesive energies and bulk moduli for β-quartz ($P6_222$).

	Experiment[a]	GGA[b]	LDA[b]	LDA[c]
a (Å)	4.9977	5.0845	5.0261	5.0526
c (Å)	5.4601	5.5647	5.5124	5.5488
c/a	1.0925	1.0944	1.0967	1.0982
V/SiO_2 (Å^3)	39.37	41.53	40.20	40.89
O(x)	0.2072	0.2091	0.2090	0.2089
Si–O	1.5895	1.6142	1.5968	1.6063
O–Si–O	110.1	109.9	109.8	
O–Si–O	111.3	110.4	110.5	
O–Si–O	107.0	108.1	108.2	
Si–O–Si	153.0	154.2	154.2	154.1
E_0 (eV/SiO_2)		−23.8242	−25.9381	
B_0 (GPa)		121.6	132.6	
B_0'		2.9	3.9	

[a] Reference [75].
[b] Present work.
[c] Reference [32].

corrections is distinctly smaller than for the more close-packed α-quartz. The axial ratios and internal parameters x are hardly influenced by the gradient corrections; agreement with experiment is excellent. A remarkable result is that the computed bulk modulus is nearly four times larger than for α-quartz (we note that our LDA result of $B_0 = 132.6$ GPa is in very good agreement with the calculation of Keskar and Chelikowsky [31] based on empirical pairwise interatomic potentials). This shows that the symmetry constraint increases the stiffness of the lattice. Experimentally, the bulk modulus of β-quartz has been measured only at the high temperature of $T = 873$ K, leading to a value of $B_0 = 56.4$ GPa, which is much smaller than the theoretical prediction [76]. The difference has to be attributed to the temperature-induced softening of the lattice due to the excitation of soft rigid-unit modes (cf. below). Both the LDA and the GGA predict the total energy to be lower for α-quartz, the structural energy differences being $\Delta E = 0.0259$ eV/SiO_2 unit (LDA) and $\Delta E = 0.0019$ eV/SiO_2 unit (GGA), corresponding to differences in the equilibrium volumes of $\Delta V = 2.9$ Å^3 (LDA) and $\Delta V = 1.34$ Å^3 (GGA). Hence although both calculations agree in predicting a driving thermodynamic potential for breaking the symmetry of the β-phase stabilized at an expanded volume, the structural differences in the equilibrium energies and volumes are sufficiently different to allow for significant differences between the microscopic scenarios of the transition established on the basis of the two approximations.

3.1.3. The $\alpha \rightarrow \beta$ phase transition in quartz. The displacive phase transition in quartz has been known of for more than a century [66], but continues to attract scientists' interest. Only less than ten years ago was it discovered that the classical $\alpha \rightarrow \beta$ transition consists in reality of two separate phase transitions, with a stable intermediate incommensurate phase that exists only over a narrow temperature interval of 1.5 K (reference [66]). The displacive $\alpha \rightarrow \beta$ phase transition is generally described within the 'soft-mode' concept for structural phase transitions [77]. The fundamental idea is that as the framework of connected SiO_4 tetrahedra buckles at the phase transition by rotations and translations of the tetrahedra, these

do not themselves distort significantly [78]. It has been shown that these soft 'rigid-unit modes' (RUM) can propagate as phonons and occur for a number of wave-vectors in the Brillouin zone and not only at the wave-vector driving the displacive phase transition [79]. The rigid-unit mode concept can also explain the occurrence of an incommensurate phase [80] and represents a unifying concept for displacive phase transitions in silicates and aluminosilicates [67]. However, there are still some unresolved problems, in particular how close to the soft-mode limit the $\alpha \rightarrow \beta$ transition really is and what the nature of the anharmonic coupling of the soft modes is. Here we make an attempt to contribute to the study of the transition by exploring the structural changes close to the transition by *ab initio* calculations.

The atomic structure was optimized at a series of fixed volumes under the symmetry constraints of either the $P6_222$ (β) or $P3_221$ (α) space groups. The structure of α-quartz becomes equivalent to that of β-quartz in the limits $u(\alpha) \rightarrow 0.5, x(\alpha) \rightarrow 2x(\beta), y(\alpha) \rightarrow x(\beta)$, $z(\alpha) \rightarrow 1/6$. Both sets of calculations have been performed using the same $3 \times 3 \times 3$ $\vec{k}$-point grid for Brillouin-zone integrations. Calculations based on a $4 \times 4 \times 4$ grid lead to identical results.

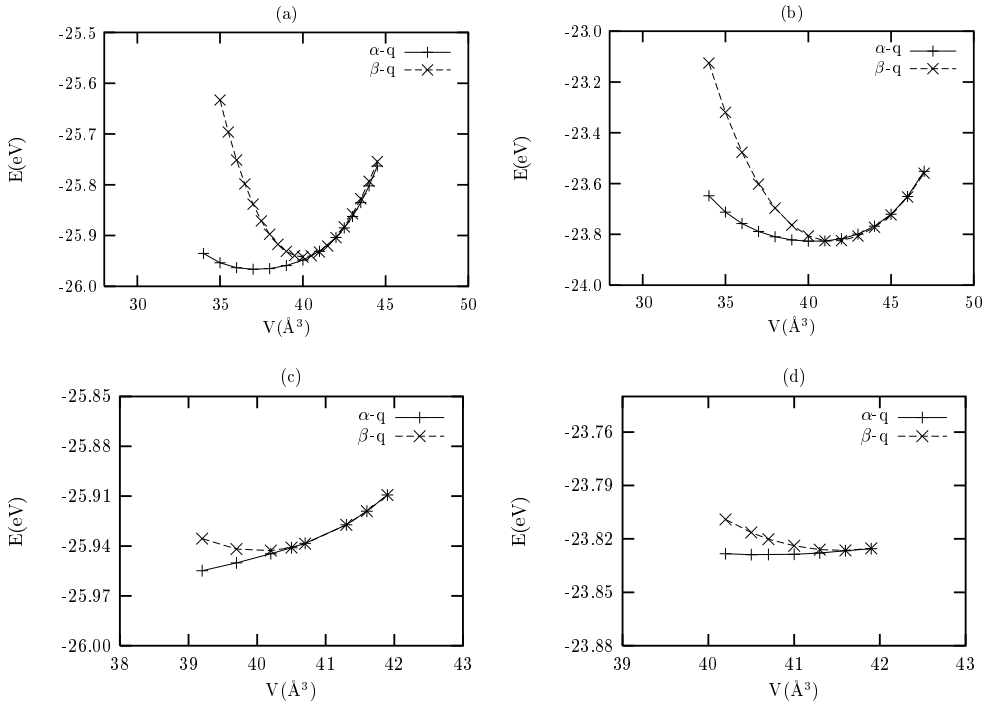

Figure 4. Energy versus volume for α- and β-quartz, calculated in the LDA (a) and in the GGA (b). Panels (c) and (d) show zooms where the two curves meet.

Figure 4 shows the variations of the total energies of α- and β-quartz with the volume. We find that the two curves merge close to the equilibrium volume of the β-phase; at larger volumes only the high-symmetry structure corresponds to an energy minimum in the configuration space fixed by the constraints of $P3_221$ space-group symmetry. Hence there is the possibility of a continuous $\alpha \rightarrow \beta$ phase transition. This is explored in more detail in figure 5 where we show the variations of the internal parameters and of the axial ratio as functions of the volume. We find that as the volume is expanded, the structural parameters of the α-phase continuously approach those of the β-phase. However, the volume for the lock-in transition beyond which

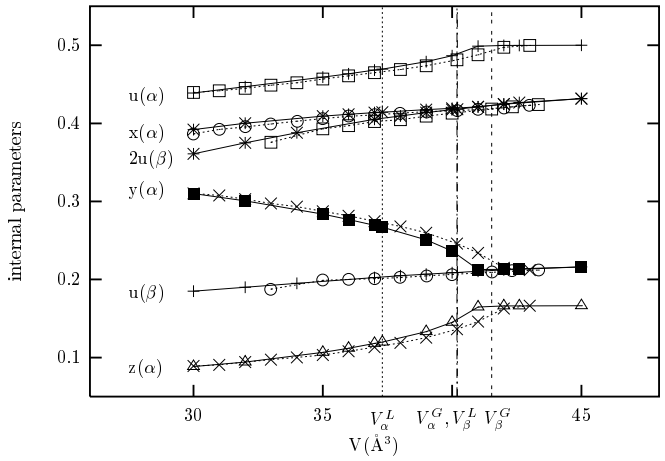

Figure 5. The variations of the internal parameters of α- and β-quartz as calculated in the LDA (full curves, squares, circles and triangles) and in the GGA (broken curves, crosses and stars). The vertical curves indicate the equilibrium atomic volumes of the α- and β-phases, respectively, calculated in the LDA (L) and GGA (G).

the α-phase does not even correspond to a metastable configuration is, in both the LDA and the GGA, predicted to be larger than the equilibrium volume of the β-phase. Hence a possible second-order $\alpha \rightarrow \beta$ phase transition at zero temperature is predicted only for small negative pressures, in agreement with the low-temperature extrapolation of the α–β coexistence line. An important result is that at fixed volume (except in the immediate neighbourhood of the lock-in transition), the optimized parameters calculated using the LDA and the GGA are identical. Hence the only effect of the GGA is to add an isotropic term to the internal pressure. This agrees with earlier results on elemental structures [81]. The examination of the energy versus volume shows that in the region where the two curves meet, the energy of the α-phase varies almost linearly with volume—hence it is almost indistinguishable from a tangent to the energy of the β-phase at the volume of the lock-in transition. Thus the hypothetical zero-temperature $\alpha \rightarrow \beta$ transition at negative pressure is second order or very weakly first order.

The variation of the local atomic geometry at the transition is examined in figure 6. Only the LDA results are shown. The tilt angle δ (which is the order parameter of the phase transformation) goes to zero at the transition. For a second-order transition, Landau theory predicts $\delta \propto (V - V_0)^{1/2}$ in the critical region where V_0 is the volume at the transition. Figure 6(a) reflects the expected behaviour of the tilt angle (see also figure 5 for the individual internal parameters). In the β-phase we find a strong decrease of the Si–O distances with decreasing volume, while the Si–O–Si bond angle varies only slightly. Below the $\beta \rightarrow \alpha$ transition the Si–O distances remain almost constant under further compression, while the Si–O–Si bond angle shows a strong decrease. Hence, in agreement with the RUM model for the displacive phase transition we find that the symmetry breaking is driven by the resistance of the SiO_4 tetrahedra to distortion and the ability of the low-symmetry structure to reduce the energetic cost of further compression by correlated rotations of the tetrahedra.

3.2. Cristobalite

'Low'- (α-) and 'high'- (β-) cristobalite form relatively open tetrahedral frameworks describable in terms of infinitely extended sheets of SiO_4 tetrahedra forming eight-membered

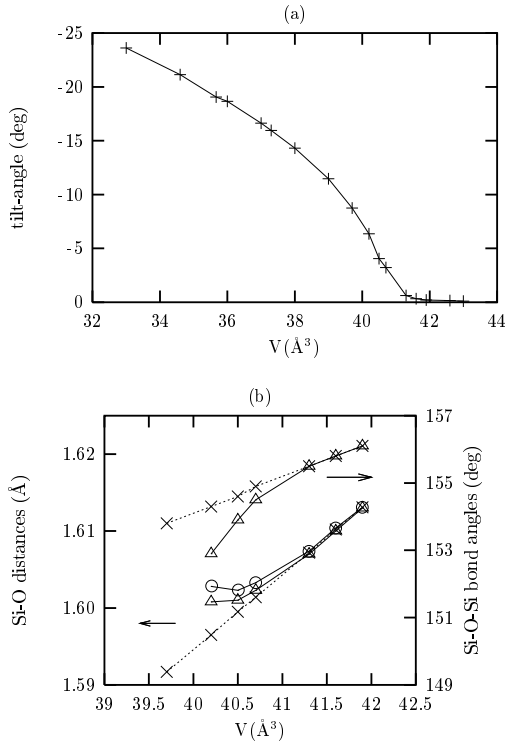

Figure 6. The variations of the tilt angle δ (a) and of the Si–O distances and of the Si–O–Si bond angle (b) close to the $\alpha \rightarrow \beta$ phase transition in quartz as calculated with the LDA. Full curves: α-quartz; broken curves: β-quartz.

rings. The structure of β-cristobalite remains controversial; at least five different structures have been proposed [82–86].

Wyckoff [82] proposed a cubic structure with space group $Fd3m$ in which the Si atoms form a diamond sublattice with the O atoms at the midpoints of the Si–Si bonds. This structure was criticized because the Si–O–Si bond angle of 180° is much larger and the Si–O distance of 1.54 Å much smaller than in any other silica polytype. Barth [83] proposed a simple cubic structure with space group $P2_13$ in which the atoms are displaced from the $Fd3m$ positions such as to yield bond distances and angles in the right range. Disorder models for 'high'-cristobalite have been proposed by Nieuwenkamp [84], Peacor [85] and Wright and Leadbetter [86]. In the model proposed by Nieuwenkamp and later refined by Peacor, the O atoms are distributed randomly over six equivalent sites forming a circle normal to the Si–Si axis such that on average the cubic $Fd3m$ symmetry is preserved. Wright and Leadbetter proposed assigning one of the six positions to the O atoms such that neighbouring SiO_4 tetrahedra are rotated relative to the ideal structure by $\pm 20^\circ$ about the $\bar{4}$ axis, leading to a tetragonal structure with $I\bar{4}2d$ symmetry. The pseudocubic $Fd3m$ symmetry of the diffraction pattern is supposed to arise from an average over small domains with the six possible orientations of the tetragonal lattice. Recently Liu *et al* [35] have examined the three structures ($Fd3m$, $P2_13$, $I\bar{4}2d$) proposed for β-cristobalite by *ab initio* total-energy calculations and claimed that the $P2_13$ structure can be discarded as being energetically disfavoured.

The structure of α-cristobalite was studied by Barth [87], Nieuwenkamp [88], Dollase [89], Pluth *et al* [90] and Downs and Palmer [91]. The structure has space group $P4_12_12$. It may be

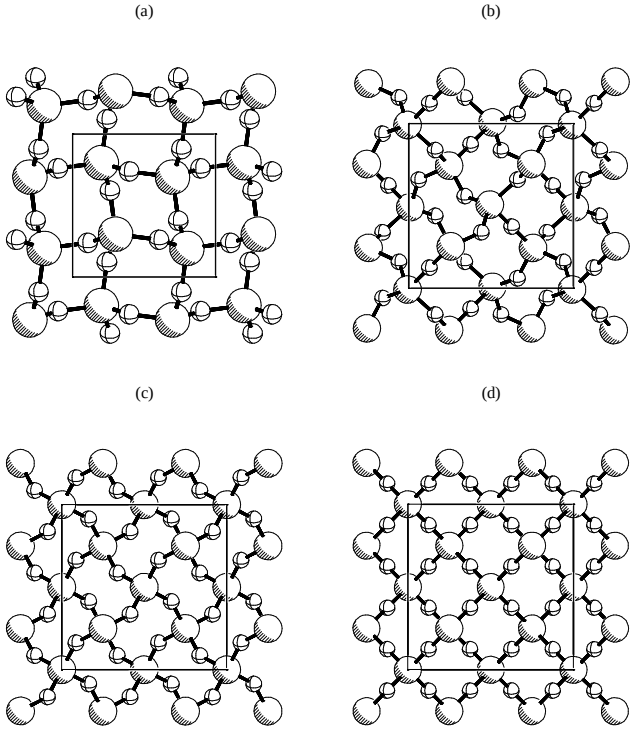

Figure 7. Representations of the crystal structures of α-cristobalite ($P4_12_12$) (a) and β-cristobalite: $P2_13$ (b), $I\bar{4}2d$ (c) and $Fd3m$ (d) structures.

considered as a distortional derivative of the ideal cubic structure of β-cristobalite. The rotation axes on neighbouring tetrahedra are orthogonal to each other (and not antiparallel as for β-cristobalite) and the rotation angles are slightly larger (about 24°). The $\alpha \rightarrow \beta$ transformation in cristobalite was investigated by Peacor [85]. It was shown that with increasing temperature the atomic positions and cell parameters of α-cristobalite relax continuously in the direction of those of the high-temperature form and that this is related to the anomalous high anisotropy of the thermal expansion of α-cristobalite. O'Keefe and Hyde [92] have pointed out that the structure of domain walls of tetragonal ($I\bar{4}2d$) β-cristobalite can be arranged such as to assume a local $P4_12_12$ symmetry. The energetics of the transformation between the two tetragonal structures of α- and β-cristobalite has been discussed by Liu *et al* [35]. The crystal structures proposed for α- and β-cristobalite are shown in figure 7.

3.2.1. α-cristobalite. In the $P4_12_12$ structure of α-cristobalite, Si occupies the Wyckoff positions (4a) with coordinates $(u, u, 0)$ and O the positions (8b) with coordinates (x, y, z). Hence at fixed volume the five independent parameters c/a, u, x, y and z must be determined. The calculations were performed for a $3 \times 3 \times 3$ grid of special points corresponding to six irreducible points. The data for the equilibrium structure obtained in the LDA and GGA are compiled in table 3, together with the experimental data of Downs and Palmer [91] for the structure and for the bulk modulus. While the LDA predicts the equilibrium volume, bond lengths and bond angles in excellent agreement with experiment, the GGA overestimates the equilibrium volume by as much as 9.8%. Despite the too-large volume, the bond distances

calculated in the GGA are almost the same as those predicted in the LDA. The expansion of the volume influences the Si–O–Si bond angle much more than the bond length. The very low bulk modulus of $B_0 = 11.5$ GPa reflects the unusual softness of the cristobalite lattice. Our present LDA results for the equilibrium volume are in very good agreement with the work of Liu *et al* [32] which is also based on ultrasoft pseudopotentials. The internal parameters calculated by Liu *et al* on the other hand are slightly less accurate, as reflected in a too-large difference in the Si–O bond length. We believe that the difference is due to the limited accuracy of a Brillouin-zone integration based on two special points only. The calculation of Teter *et al* [33] based on extended norm- and hardness-conserving pseudopotentials on the other hand overestimates the equilibrium volume by as much as 6.1%. We believe that the difference is due to the use of hard pseudopotentials for which complete plane-wave convergence is almost impossible to achieve.

Table 3. Structural parameters, bond lengths (in Å), bond angles (in degrees), cohesive energies and bulk moduli for α-cristobalite ($P4_12_12$). δ is the tilt angle of the SiO_4 tetrahedra relative to their orientation in the high-symmetry form ($Fd3m$) of β-cristobalite.

	Experiment[a]	GGA[b]	LDA[b]	LDA[c]	LDA[d]
a (Å)	4.9717	5.1190	4.9751	5.0630	4.9586
c (Å)	6.9222	7.1683	6.9261	7.0823	6.9074
c/a	1.3923	1.4003	1.3921	1.3988	1.3930
V/SiO_2 (Å^3)	42.77	46.96	42.86	45.39	42.46
Si(u)	0.3003	0.2869	0.2988	0.2895	0.3028
O(x)	0.2392	0.2439	0.2399	0.2431	0.2383
O(y)	0.1044	0.0777	0.1007	0.0833	0.1093
O(z)	0.1787	0.1657	0.1768	0.1687	0.1816
Si–O	1.6026	1.6144	1.5970	1.6037	1.6046
Si–O	1.6034	1.6146	1.5991	1.6037	1.6113
O–Si–O	109.0	108.7	109.1	108.7	109.1
O–Si–O	110.0	109.6	109.9	109.7	110.0
O–Si–O	108.2	108.8	108.3	108.7	108.0
O–Si–O	111.4	111.2	111.1	111.4	111.7
Si–O–Si	146.5	154.2	147.7	152.2	144.9
δ	23.25	18.03	22.5		
E_0 (eV/SiO_2)		−23.8579	−25.9388		
B_0 (GPa)	11.5	9.4	12.8	11.9	14.8
B_0'	9	3.8	6.3	3.0	2.4

[a] Reference [91].
[b] Present work.
[c] Reference [33].
[d] Reference [32].

The unusual softness of the structure of α-cristobalite leads one to expect large structural variations as functions of volume. Indeed as shown in figure 8 we find a continuous trend towards the cubic $Fd3m$ symmetry on expansion expressed by $c/a \to \sqrt{2}$, $u(\mathrm{Si}) \to 1/4$, $x(\mathrm{O}) \to 1/4$, $y(\mathrm{O}) \to 0$ and $z(\mathrm{O}) \to 1/8$. At a fixed volume, LDA and GGA result again in almost identical structural parameters, except in the immediate neighbourhood of the tetragonal-to-cubic transition which occurs at volumes of $V = 50.45$ Å^3/SiO_2 unit (LDA) and $V = 53$ Å^3/SiO_2 unit (GGA). The change in the structure affects only the Si–O–Si bond angle (which tends towards 180°), while the Si–O bond lengths remain almost constant over a very

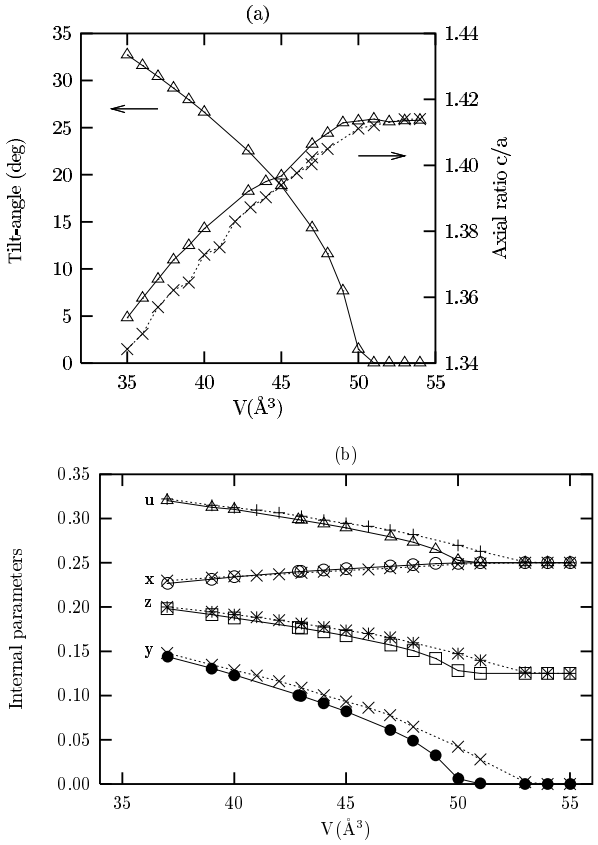

Figure 8. The variations of the axial ratio c/a and of the tilt angle δ of the SiO_4 tetrahedra (a) and of the internal parameters u, x, y, z of α-cristobalite ($P4_12_12$) (b) with volume. $c/a = \sqrt{2}$, $u = x = 1/4$, $y = 0$, $z = 1/8$ correspond to the cubic ($Fd3m$) limit. Full curves, triangles, squares and circles represent LDA results; broken curves, crosses and stars crosses represent GGA results.

wide range of volumes, the differences between the two inequivalent distances decreasing on approaching the high-symmetry structure (see figure 9). We note that this trend agrees with the observations of Peacor [85] on the structural variations of α-cristobalite with increasing temperature.

3.2.2. β-cristobalite. The three crystal structures proposed for β-cristobalite ($P2_13$, $I\bar{4}2d$, $Fd3m$) can in principle be studied using a common simple cubic cell containing eight SiO_2 units, although a smaller cell with only four formula units would be sufficient for the last two structures. In the simple cubic $P2_13$ structure, Si occupies Wyckoff positions (4a) with coordinates (u, u, u), $u = 0.255$ for Si1 and $u = -0.008$ for Si2, and O atoms Wyckoff positions (4a) with $x = 0.125$ (O1) and (12b) with coordinates (x, y, z), $x = y \approx 0.66$, $z \approx 0.06$ (O2) (after reference [87]). The 'ideal' cristobalite structure with $Fd3m$ symmetry is recovered in the limit $u(\mathrm{Si1}) \to 1/4$, $u(\mathrm{Si2}) \to 0$, and $x \to y \to 5/8$, $z \to 1/8$ for O2. In the tetragonal $I\bar{4}2d$ structure the axial ratio deviates only slightly from the value $c/a = \sqrt{2}$ for which the doubled cell becomes cubic. Si atoms occupy Wyckoff positions (4a) in the tetragonal $I\bar{4}2d$ cell (corresponding to the ideal $Fd3m$ positions in the limit $c/a \to \sqrt{2}$).

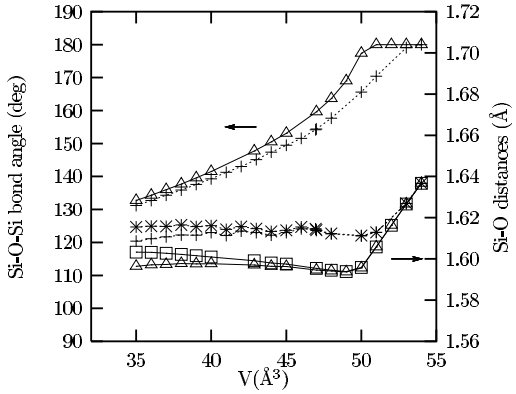

Figure 9. The variations of the Si–O bond lengths and of the Si–O–Si bond angle of α-cristobalite. The key to the symbols is the same as for figure 8.

The O atoms occupy positions (8d) with coordinates $(x, 1/4, 1/8)$ and $x = 0.079$. $Fd3m$ symmetry is recovered in the limit $x \to 0$. If, neglecting the small tetragonal strain, the structure is set up in the doubled cubic cell (rotated by 45° around the tetragonal axis), the Si positions are compatible with $P2_13$ symmetry, but the O positions are not. Hence a possible $P2_13 \leftrightarrow I\bar{4}2d$ transformation implies a change of the Wyckoff positions of the O atoms and not only a mere change of the internal parameters as for the $I\bar{4}2d \to Fd3m$ transition.

The optimized internal parameters are summarized in table 4. For both the $P2_13$ and $I\bar{4}d2$ phases, the LDA equilibrium volume is in good agreement with experiment, whereas for the idealized $Fd3m$ structure a much larger equilibrium volume is predicted. For the $I\bar{4}d2$ structure, the calculated Si–O distances agree with experiment within an error of 0.014 Å; the O–Si–O bond angles are accurate to within 2°. A larger error of 5.2° is found for the Si–O–Si angle. For the $P2_13$ lattice on the other hand, our optimized structure is much closer to a network of regular tetrahedra than the experimental structure of Barth [83]. We think

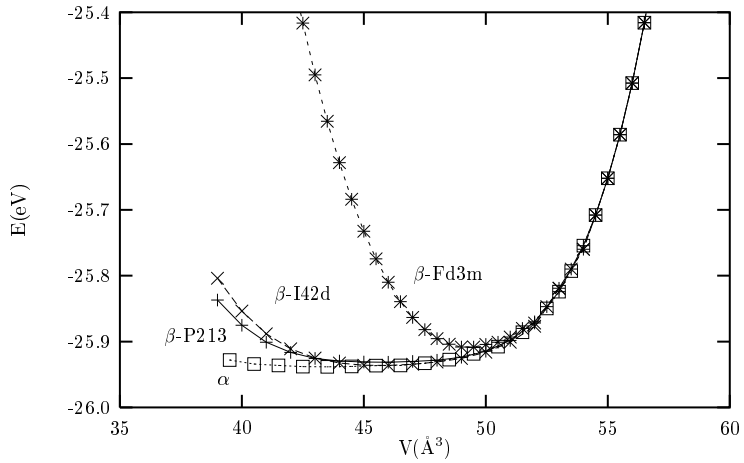

Figure 10. The variations of the total energies of α-cristobalite ($P4_12_12$) and β-cristobalite ($P2_13$, $I\bar{4}2d$ and $Fd3m$) with volume.

Table 4. Structural parameters, bond lengths (in Å), bond angles (in degrees), cohesive energies and bulk moduli for β-cristobalite assuming $P2_13$, $I\bar{4}2d$ or $Fd3m$ symmetry.

(a) $P2_13$

	Experiment[a]	GGA	LDA
a (Å)	7.159	7.2679	7.13
V/SiO_2 (Å^3)	45.86	47.99	45.31
Si1(u)	0.255	0.2722	0.2758
Si2(u)	−0.008	0.0168	0.0184
O1(x)	0.125	0.1443	0.1470
O2(x)	0.66	0.6388	0.6391
O2(y)	0.66	0.6502	0.6552
O2(z)	0.06	0.0645	0.0557
Si1–O1	1.6120	1.6101	1.5912
Si1–O2	1.6084	1.6155	1.5964
Si2–O1	1.6492	1.6059	1.5872
Si2–O2	1.6641	1.6158	1.5984
O2–Si1–O2	101.3	109.2	108.9
O1–Si1–O2	116.7	109.7	110.0
O2–Si2–O2	119.2	109.8	109.8
O1–Si2–O2	95.1	109.2	109.1
Si1–O2–Si2	137.2	154.2	150.6
Si1–O1–Si2	180	180	180
E_0 (eV/SiO_2)		−23.8575	−25.9316
B_0 (GPa)	16	12.5	14.0
B_0'		4.2	7.1

(b) $I\bar{4}d2$ and $Fd3m$

		$I\bar{4}2d$		$Fd3m$	
	Experiment[b]	GGA	LDA	GGA	LDA
a (Å)	7.131	7.226	7.1153	7.417	7.352
c/a		1.0146	1.0186		
V/SiO_2 (Å^3)	45.33	47.85	45.86	51.01	49.67
O(x)	0.079	0.0896	0.0862		
Si–O	1.611	1.6131	1.5984	1.6059	1.5918
O–Si–O	107.8	108.8	108.7	109.5	109.5
O–Si–O	112.9	110.8	110.9		
Si–O–Si	146.7	154.1	151.8	180	180
E_0 (eV/SiO_2)		−23.8636	−25.9375	−23.8396	−25.9036
B_0 (GPa)		21.7	27.77	119.5	128.6
B_0'		3.8	5.1	4.3	4.9

[a] Reference [87].
[b] Reference [86]. (The experimental data refer to the $I\bar{4}2d$ setting.)

that the large differences in the Si–O distances (up to 0.065 Å) and in the tetrahedral angles (up to 14°), as well as the exceptionally low Si–O–Si bond angle of 137.2°, are unrealistic. Energetically we find the low-symmetry variants to be degenerate within the accuracy of our

calculations ($\Delta E \leqslant 6$ meV/SiO_2), but lower in energy than the high-symmetry structure by $\approx$34 meV/SiO_2. Note that the energetic degeneracy of the $P2_13$ and $I\bar{4}d2$ phases depends on a careful optimization with respect to all parameters.

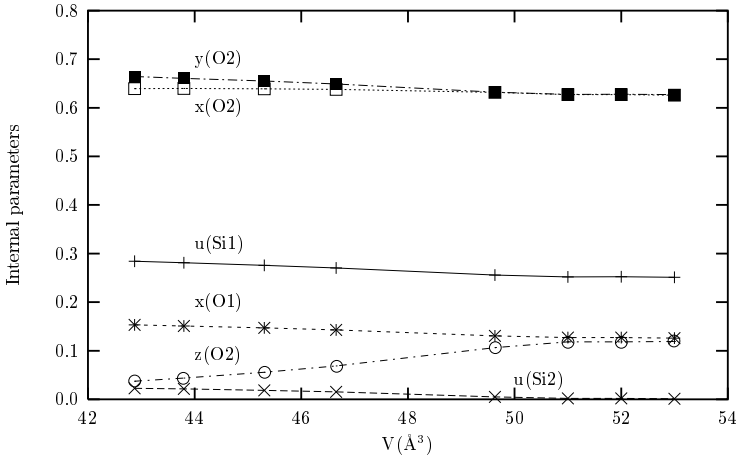

Figure 11. The variations of the internal parameters u(Si1), u(Si2), x(O1), x(O2), y(O2) and z(O2) of β-cristobalite ($P2_13$) with volume calculated with the LDA. $y(\mathrm{O2}) = x(\mathrm{O2}) = \frac{5}{8}$, $x(\mathrm{O1}) = z(\mathrm{O2}) = \frac{1}{8}$, $u(\mathrm{Si1}) = \frac{1}{4}$ and $u(\mathrm{Si2}) = 0$ correspond to the limiting $Fd3m$ structure.

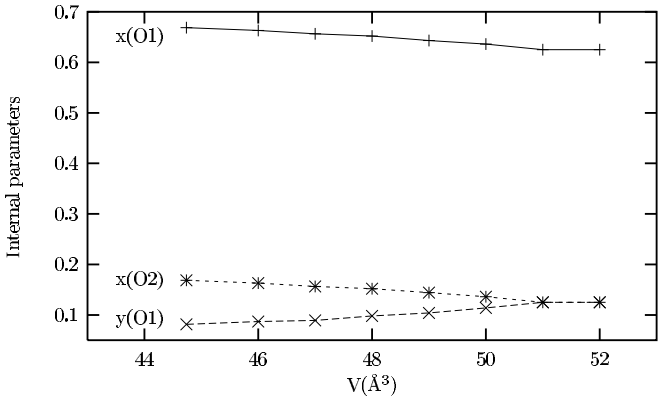

Figure 12. The variations of the internal parameters x(O1), x(O2) and y(O1) of β-cristobalite ($I\bar{4}2d$) with volume. LDA results only. $x(\mathrm{O2}) + \frac{1}{2} = x(\mathrm{O1}) = \frac{5}{8}$ and $y(\mathrm{O1}) = x(\mathrm{O2})$ correspond to the limiting $Fd3m$ structure.

Figure 10 shows the optimized total energy of all three structural variants as a function of volume. The calculations have been performed using the same $3 \times 3 \times 3$ grid as for α-cristobalite. This is the central result of our study of β-cristobalite. We find that at volumes larger than about 51 Å^3/SiO_2 unit both the simple cubic $P2_13$ and the tetragonal $I\bar{4}2d$ structures relax to face-centred $Fd3m$. In the range between 45 Å^3 and 51 Å^3 the optimized $P2_13$ and $I\bar{4}2d$ structures are energetically degenerate (but not structurally identical); at volumes lower than 45 Å^3 the $P2_13$ structure is favoured. Figures 11 and 12 show the variations of the internal parameters of the two structures as functions of volume—in both cases we find a continuous transition to the high-symmetry $Fd3m$ structure. Figure 13 shows for the $P2_13$ structure the

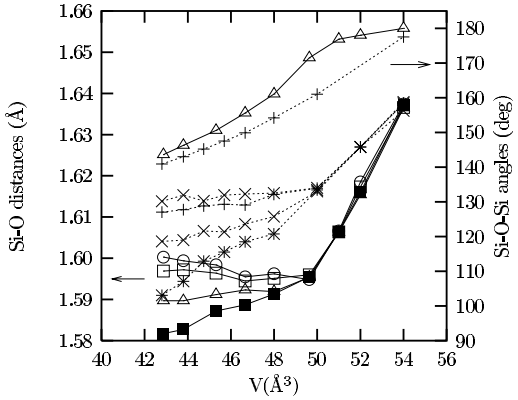

Figure 13. The variations of the Si–O bond lengths and of the Si–O–Si bond angles in β-cristobalite ($P2_13$) with volume. Full curves, triangles, squares and circles: LDA; broken curves, crosses and stars: GGA.

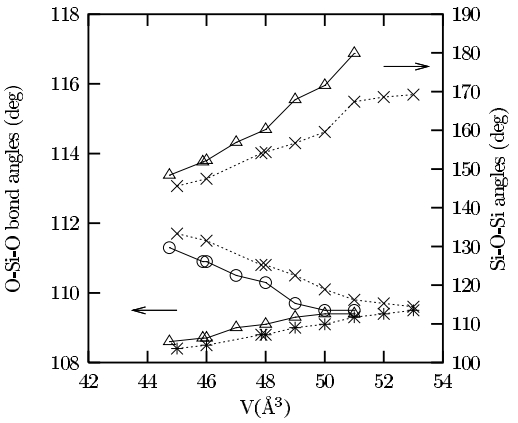

Figure 14. The variations of the O–Si–O and of the Si–O–Si bond angles in β-cristobalite ($I\bar{4}2d$) with volume.

variations of the Si–O bond lengths and of the Si–O–Si angles with volume and figure 14 the variations of the Si–O–Si and O–Si–O angles for the $I\bar{4}2d$ structure with volume. The important result is that, as in the case of α-cristobalite, the tetrahedral O–Si–O angles remain almost constant while the Si–O–Si angles are strongly volume dependent. The Si–O bond lengths show only little variation, the differences between the inequivalent Si–O distances in the $P2_13$ structure decreasing on expansion. Note that the differences in the bond lengths have already vanished before the Si–O–Si angle reaches the value of 180° characteristic for the high-symmetry structure. Thus the breaking of the $Fd3m$ symmetry results from the stiffness of the SiO_4 units under compression. We also find, as for the other structures, that the LDA leads to an accurate prediction of the volume, while the GGA leads to a ∼5% overestimate. At fixed volume, the structural predictions of LDA and GGA are identical.

Our result that on expansion the $I\bar{4}2d$ structure relaxes towards the 'ideal' $Fd3m$ symmetry agrees with the conclusions of Liu *et al* [35]. However, Liu *et al* found that the $P2_13$ symmetry should have a much higher energy. The discrepancy could be due to an insufficient structural optimization or to the restriction of the Brillouin-zone integration to a single $\vec{k}$-point.

3.2.3. The $\alpha \rightarrow \beta$ transition in cristobalite. Figure 10 shows the variations of the total energies of the $\alpha(P4_12_12)$, $\beta(P2_13$ or $I\bar{4}2$d) and ideal—$\beta(Fd3m)$ phases with volume. The α-phase is lower in energy than the β-phase by only 0.0012 eV/SiO_2 unit in the LDA; however, in the GGA the β-phase is lower by 0.0056 eV/SiO_2 unit. The important result is that the α-cristobalite structure and the two structural variants of β-cristobalite can be energetically almost degenerate over a rather wide range of densities.

Various scenarios have been developed for the mechanism of the phase transition. According to O'Keefe and Hyde [92], the $\alpha \rightarrow \beta$ transition in cristobalite can be described in terms of a rotation of the tetrahedra by a tilt angle δ, in analogy to the $\alpha \rightarrow \beta$ transition in quartz. In the most general case allowed for the α-phase, the SiO_4 tetrahedra are not regular, their symmetry being reduced from T_d to C_2 (with the twofold axis parallel to [110] in the basal plane). The tilt angle measures the rotations about this axis; in the limit of regular tetrahedra the change in all lattice parameters can be expressed in terms of the tilt angle. Compared to that for α-quartz, the tilt angle in 'low'-cristobalite is substantially larger (δ(exp) $= 24.8^\circ$ according to reference [90]; δ(theor) $= 22.5^\circ$). Our results for the internal parameters as functions of volume (see figure 8) demonstrate that at expanded volume there is the possibility of a continuous $\alpha(P4_12_12) \rightarrow \beta(Fd3m)$ transition, but the barrier for the relaxation of the α-phase into the β-phase actually vanishes only at volumes lower than the equilibrium volume of the high-symmetry phase. As for the $\alpha \rightarrow \beta$ transition in quartz, we find that the calculated variations of the axial ratio and tilt angle δ close to the transition conform with the expectations of Landau theory ($c/a \propto (V - V_0)$, $\delta \propto (V - V_0)^{1/2}$, where V_0 is the volume at the transition).

Again the mechanism for the $\alpha \rightarrow \beta$ transition can be interpreted in terms of the RUM concept. In β-cristobalite a large number of RUMs have been identified [93]. The RUM at the X point (symmetry X_4) gives rise to both the translations and the rotations of the tetrahedra required to produce the α-phase, the amplitude of the RUM being proportional to the tilt angle δ. The $I\bar{4}d2$ structure can be generated from the ideal $Fd3m$ structure by condensation of the Γ_5^- zone-centre RUM [93]. The important result of the present study is that all structures describable in terms of a condensation of RUMs of the idealized β-cristobalite structure are energetically degenerate over a substantial range of densities (between 45 and 50 $Å^3/SiO_2$; see figure 10), but at volumes below $\approx$43 $Å^3$ the α-phase is energetically preferred over the distorted β-variants. These structures have been described either as truly dynamically disordered phases (with random structural fluctuations describable in terms of a condensation of RUMs) or as composed of static domains of the distorted phases. The energetic degeneracy demonstrated by our calculations argues against a static multidomain model [35, 86] and also against dynamically disordered models assuming a hopping of the O atoms between symmetry-equivalent positions. Such a scenario would require that the dynamic behaviour is dominated by a single RUM (in this case the soft X_4 phonon). Our result, however, suggests the presence of many energetically equivalent RUMs and explains the observed similarity of the dynamical properties of β-cristobalite with those of amorphous silica and other orientationally disordered crystals: the common feature is a potential energy surface with a large number of local minima of comparable depth.

3.3. Tridymite

Tridymites are low-density polymorphs of silica occurring in a variety of different crystal structures. The structure of ideal high-temperature (β-) tridymite is closely related to the ideal β-cristobalite structure (cf. the classification of Dmitriev *et al* [65]). The basic building blocks are sheets of SiO_4 tetrahedra arranged in hexagonal rings. Rings in successive sheets are directly superposed, with the result that large open pipes are formed perpendicular to the sheets

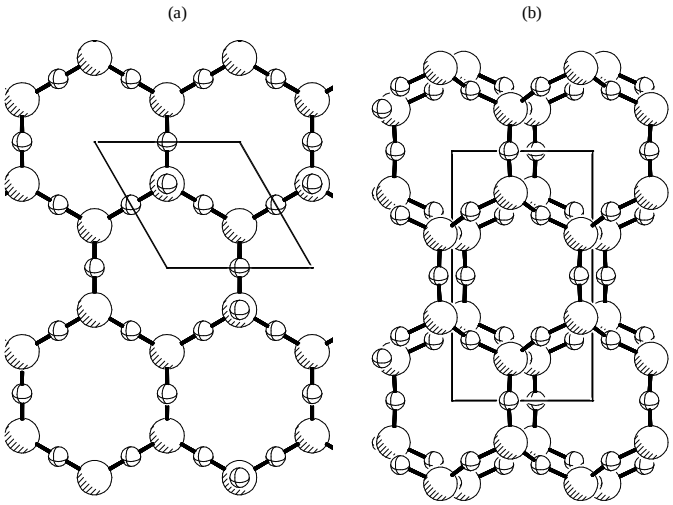

Figure 15. Representations of the crystal structures of idealized (space group $P6_3/mmc$) (a) and orthorhombic (space group $C222_1$) (b) tridymite.

(figure 15) and related by a mirror symmetry. Hence in β-tridymite the stacking sequence of the layers of tetrahedra is ABAB$\cdots$ [49], whereas in idealized ($Fd3m$) β-cristobalite the stacking sequence is ABCABC$\cdots$ along the [111] axis of the cubic cell [82, 85]. The space-group symmetry of idealized β-tridymite is $P6_3/mmc$; Si atoms occupy positions (4f) with coordinates $(1/3, 2/3, w)$ and $w = 0.0620$, O1 atoms positions (2c) with coordinates $(1/3, 2/3, 1/4)$ and O2 atoms occupy positions (6g) with coordinates $(1/2, 0, 0)$ (after reference [49]). Kihara (references [49,94]) also discussed a model with split oxygen positions for ideal tridymite leading to an orthorhombic ($Cc2m$) cell with $a = \sqrt{3}a_h$, $b = b_h$, $c = c_h$ (the subscript referring to the hexagonal cell) and eight formula units per cell. At decreasing temperature, the crystal symmetry of tridymite is gradually lowered to orthorhombic $C222_1$ (reference [95]), $P2_12_12_1$ (reference [96]), monoclinic Cc (references [97, 98]) and finally triclinic (reference [49]). The monoclinic cell described by Kato and Nukui [98] contains 48 formula units and the triclinic cell of Konnert and Appleman [99] 320 formula units. The present study is restricted to the hexagonal and orthorhombic ($C222_1$) high-temperature forms. In the ideal hexagonal structure at fixed volume only the axial ratio and the internal parameter w have to be determined. The calculations have been performed with a $3 \times 3 \times 3$ grid of $\vec{k}$-points, corresponding to eight irreducible points. The results are summarized in table 5. Surprisingly, the LDA predicts an equilibrium volume that is 9.5% larger than the experimental volume calculated from the lattice parameters of Kihara [49], measured at a high temperature of $T = 733$ K. The GGA volume is 13.2% greater than the experimental volume. The axial ratio and internal parameter on the other hand are almost identical to the experimental values and nearly independent of the volume.

In the orthorhombic $C222_1$ structure of β-tridymite, the Si atoms occupy Wyckoff positions (8c) with coordinates (u, v, w). Oxygen atoms are located at positions (4a) with coordinates $(x, 0, \frac{3}{4})$, O2 atoms at positions (4b) with coordinates $(0, y, \frac{1}{2})$ and O3 atoms at positions (8c) with coordinates (x, y, z). The idealized hexagonal structure of β-tridymite is recovered in the limit $u(\mathrm{Si}) \to \frac{1}{6}$, $v(\mathrm{Si}) \to \frac{1}{2}$, $w \to \frac{7}{16}$, $x(\mathrm{O1}) \to \frac{1}{3}$, $y(\mathrm{O2}) \to \frac{1}{2}$, $x(\mathrm{O3}) \to y(\mathrm{O3}) \to \frac{1}{4}$, $z(\mathrm{O3}) \to \frac{1}{2}$. In the orthorhombic structure, pairs of SiO_4 tetrahedra joined at the O1 sites are alternately tilted by $\delta = \pm 8^\circ$ relative to the c-axis, resulting in a

Table 5. Structural parameters, bond lengths (in Å), bond angles (in degrees), cohesive energies and bulk moduli for hexagonal β-tridymite ($P6_3/mmc$).

	Experiment[a]	GGA	LDA
a (Å)	5.035, 5.052	5.2484	5.1908
c (Å)	8.220, 8.27	8.5683	8.4702
c/a	1.632, 1.637	1.632	1.6317
V/SiO_2 (Å^3)	45.11, 45.39	51.10	49.41
Si(w)	0.062	0.0624	0.0624
Si–O	1.555	1.6068	1.5889
Si–O	1.546	1.6064	1.5886
O–Si–O	109.4	109.5	109.5
O–Si–O	109.7	109.4	109.5
E_0 (eV/SiO_2)		−23.8446	−25.9194
B_0 (GPa)		130.5	139.59
B_0'		3.14	4.7

[a] References [6, 49].

slight flexure of the tetrahedra sharing a triangular face formed by the O2 and O3 atoms. In the hexagonal phase these tetrahedra are aligned along the c-axis. The distortion results in Si–O–Si angles around O2 and O3 that are significantly lower than 180°, but still large compared to the normal values found in quartz (143.7° in the α-phase, 153.0° in β-quartz) and cristobalite (146.5° (α), 146.6° (β-$I\bar{4}d2$)). The bond distances are also substantially smaller (weighted average: 1.56 Å) than in quartz or cristobalite.

The structural optimization in the LDA predicts a very accurate equilibrium volume, but the calculated Si–O bond lengths are on average ≈0.03 Å larger than found in the experiment. The larger Si–O distances are compensated by a larger deviation of the Si–O–Si bond angles from the idealized value of 180°. This concerns in particular the Si–O3–Si angle where we calculate a value of 150.4° compared to the experimental result of 165.2° (see table 6). In the GGA we find again a larger equilibrium volume, but essentially the same structure at fixed volume. At equilibrium, the structural energy difference is 11 meV/SiO_2 unit in the LDA, but only 4 meV in the GGA (the orthorhombic structure being lower in energy). As for quartz and cristobalite, we note on expansion a continuous convergence of all structural parameters of orthorhombic tridymite towards the limiting values defining the hexagonal structure. The variations of the tilt angle δ and of Si–O3–Si bond angle in the orthorhombic phase are shown in figure 16. Figure 17 shows the variations of the total energies in the two phases with volume. The two diagrams taken together demonstrate the possibility of a continuous phase transition at expanded volumes. However, figure 16 illustrates also the difficulties associated with *ab initio* structural optimizations close to a second-order phase transition. According to Landau theory, the tilt angle (the order parameter of the transition) should vary as $\delta \propto (V - V_0)^{1/2}$. The calculated values follow roughly the expected behaviour, but we find it difficult to relax the low-symmetry phase exactly to $\delta = 0$ characteristic for the high-symmetry phase. The reason for this is that the restoring forces are very small. To obtain an exactly converged result, all parameters of the calculation (cut-off values for total energies, forces, number of $\vec{k}$-points etc) would have to be set to extreme values, resulting in a very high computational effort.

In view of the very good agreement between the LDA and experiment ($\Delta V \leqslant 2\%$) for both the 'low'- and 'high'-forms of quartz and cristobalite (and also for keatite, coesite and stishovite; see below), the disagreement that we find for both hexagonal and orthorhombic

Table 6. Structural parameters, bond lengths (in Å), bond angles (in degrees), cohesive energies and bulk moduli for orthorhombic tridymite ($C222_1$). δ is the tilt angle of the SiO_4 tetrahedra relative to their orientation in hexagonal β-tridymite (in degrees).

	Experiment[a]	GGA	LDA
a (Å)	8.74	9.1132	8.9766
b (Å)	5.05	5.0960	5.0084
c (Å)	8.24	8.3459	8.1786
c/a	0.9427	0.9158	0.9111
b/a	0.5778	0.5591	0.5579
V/SiO_2 (Å^3)	45.46	48.45	45.96
Si(u, v, w)	0.1684, 0.5358, 0.4385	0.1669, 0.5734, 0.4373	0.1671, 0.5821, 0.4374
O1(x, y, z)	0.3336, 0.0, 0.75	0.3302, 0.0, 0.75	0.3301, 0.0, 0.75
O2(x, y, z)	0.0, 0.5597, 0.5	0.0, 0.5839, 0.5	0.0, 0.5961, 0.5
O3(x, y, z)	0.2547, 0.3029, 0.5213	0.2587, 0.3588, 0.5388	0.2576, 0.3693, 0.5435
Si–O1	1.5644	1.6088	1.5868
Si–O2	1.5615	1.6093	1.5866
Si–O3	1.5530	1.6159	1.5965
O1–Si–O2	108.7	109.8	109.6
O1–Si–O3	110.7	110.4	110.2
O2–Si–O3	111.9	109.9	109.6
Si–O1–Si	178.7	178.0	178.2
Si–O2–Si	171.2	176.2	175.1
Si–O3–Si	165.2	152.2	150.4
δ	8	11.3	13.5
E_0 (eV/SiO_2)		−23.8485	−25.9302
B_0 (GPa)		25.4	30.8
B_0'		2.3	4.1

[a] Reference [95].

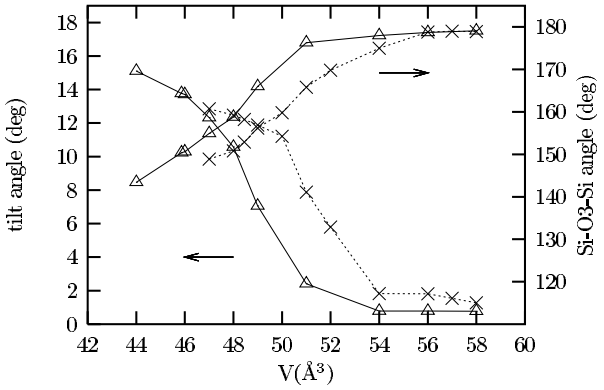

Figure 16. The variations of the tilt angle and of the Si–O3–Si bond angle in orthorhombic tridymite with volume. $\delta = 0^\circ$ and Si–O3–Si $= 180^\circ$ correspond to the limiting structure of hexagonal tridymite. Full curves and triangles: LDA; broken curves and crosses: GGA.

tridymite is certainly surprising. To the best of our knowledge, no previous LDA calculations have been performed on this system. A calculation based on empirical pair potentials by Keskar

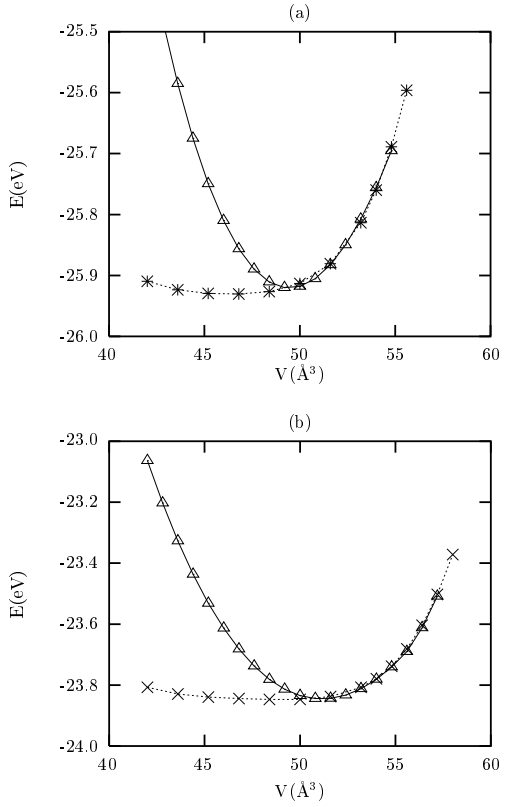

Figure 17. The energy–volume relations for hexagonal and orthorhombic tridymite calculated using the LDA (a) and GGA (b). Triangles and full curves: hexagonal tridymite; open symbols and broken curves: orthorhombic tridymite.

and Chelikowsky [31] predicts a volume even larger than our GGA result. The experimental structure ascribed to ideal hexagonal β-tridymite is also surprising because:

(a) It leads to the same short Si–O bond length of 1.54 Å and Si–O–Si bond angles of 180° as have already been criticized in Wyckoff's [82] original proposal of a cubic structure for β-cristobalite. Unlike in all other structures, the Si–O bond lengths vary strongly under compression, while the bond angles remain fixed by symmetry.

(b) The LDA predictions for the equilibrium volume of β-tridymite (ABAB$\cdots$ stacking sequence) and β-cristobalite with $Fd3m$ symmetry (ABCABC$\cdots$ stacking sequence) differ only by about 0.3 Å^3/SiO_2 unit; the structural energy difference is ΔE(β-cristobalite − hexagonal β-tridymite) $\sim$ 0.015 eV (LDA) or $\sim$0.005 eV (GGA)—hence the predictions are consistent in view of the close structural relationship.

(c) The calculation predicts a very large bulk modulus of $B_0 = 139.6$ GPa, i.e. ten times larger than for the denser cristobalite phases and even larger than that of β-quartz which has the lowest compressibility of all silica polymorphs. Only for the cubic 'ideal' β-cristobalite do we find a similar value. Such a high value can only be the result of symmetry constraints.

In the distorted orthorhombic form, the Si–O distances predicted by the LDA are 0.02 to 0.04 Å larger than found in the experiment; at the almost correct density, this is possible only at the expense of stronger distortions of the Si–O3–Si angle. Dollase [95] has attempted to reconcile

the short apparent Si–O distances in orthorhombic tridymite with the known stiffness of the Si–O bonds in terms of correlated atomic motions of the oxygens (with highly anisotropic thermal ellipsoids for the O atoms 'riding on silicon'). Our calculations confirm that in the static structure of orthorhombic tridymite, the Si–O distances are under considerable strain. This strain can be released only by a further lowering of the crystalline symmetry. At the moment, a better understanding of the structures of 'low'-tridymite must be left to future investigations.

3.4. Keatite

Keatite is a polymorph of silica with a density intermediate between those of α-cristobalite and β-quartz. It appears not to have a field of thermodynamic stability, but may be synthesized by crystallization at moderate temperature (200 °C to 400 °C) and pressures (2 to 3 kbar). Keatite is also found, although rarely, in nature [50].

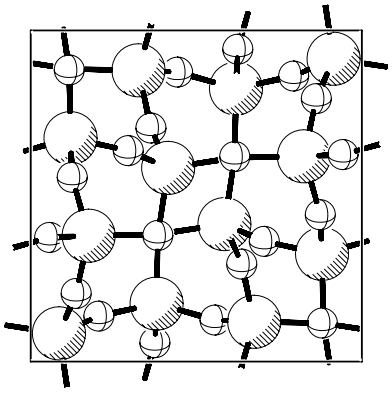

Figure 18. A representation of the crystal structure of keatite (space-group symmetry $P4_12_12$).

The structure consists of corner-sharing tetrahedra forming fivefold, sevenfold and eightfold rings (see figure 18). The space-group symmetry is $P4_12_12$, like for α-cristobalite. The primitive cell contains twelve SiO_2 units. Si1 atoms occupy positions (4a) with coordinates $(u, u, 0)$ and Si2 atoms occupy positions (8b) with coordinates (u, v, w); O1, O2 and O3 atoms occupy positions (8b) with coordinates (x, y, z). The values of the internal parameters are given in table 7. At fixed volume, fourteen independent structural parameters have to be determined. The calculations have been performed on a $3 \times 3 \times 3$ $\vec{k}$-point grid corresponding to six irreducible points.

The equilibrium volume calculated within the LDA differs from the experimental value by only 0.6%; the axial ratio is also correctly predicted. The GGA overestimates the volume by 6.5% and leads also to a slightly larger axial ratio. If the volume is varied, the lattice constant a remains almost constant. The expansion leads to a pronounced elongation of the tetragonal cell. Again, LDA and GGA yield identical structures at a given volume (see figure 19). Hence we can expect a pronounced anisotropy of the thermal expansion, as in α-cristobalite with the same space-group symmetry. The equilibrium volume and total energy of keatite are slightly lower than those of β-quartz, but larger than those of α-quartz. The relatively large bulk modulus is also intermediate between those of the two quartz polymorphs. The optimized structural parameters, as well as the bond lengths and angles, are in good agreement with experiment (see table 7).

Table 7. Structural parameters, bond lengths (in Å), bond angles (in degrees), cohesive energies and bulk moduli of keatite ($P4_12_12$).

	Experiment[a,b]	GGA	LDA
a (Å)	7.464	7.5646	7.4669
c (Å)	8.620	8.9333	8.5639
c/a	1.1548	1.1809	1.1469
V/SiO_2 (Å^3)	40.02	42.6	39.79
Si1(u)	0.4100	0.4217	0.4150
Si2(u, v, w)	0.3260, 0.1200, 0.2480	0.3315, 0.1234, 0.2333	0.3251, 0.1199, 0.2496
O1(x, y, z)	0.4450, 0.1320, 0.4000	0.4568, 0.1192, 0.3785	0.4433, 0.1252, 0.4037
O2(x, y, z)	0.1170, 0.1230, 0.2960	0.1282, 0.1115, 0.2869	0.1191, 0.1162, 0.2976
O3(x, y, z)	0.3440, 0.2970, 0.1430	0.3623, 0.3074, 0.1443	0.3628, 0.2944, 0.1467
Si1–O2	1.6140	1.6162	1.5952
Si1–O3	1.5727	1.6163	1.5943
Si2–O1	1.5854	1.6067	1.5888
Si2–O2	1.5701	1.6136	1.5921
Si2–O3	1.6070	1.6197	1.5975
O2–Si1–O3	114.2	110.4	110.6
O3–Si1–O3	106.2	109.8	107.6
O1–Si2–O1	112.1	108.5	108.6
O1–Si2–O2	109.2	108.7	108.8
O1–Si2–O3	111.8	109.2	109.9
O2–Si2–O3	102.3	109.3	109.1
Si2–O1–Si2	155.8	157.6	153.1
Si2–O2–Si1	149.3	150.4	149.3
Si1–O3–Si2	155.3	153.0	159.8
E_0 (eV/SiO_2)		−23.8282	−25.9416
B_0 (GPa)		48.6	52.2
B_0'		3.87	4.47

[a] Reference [6].
[b] Reference [50].

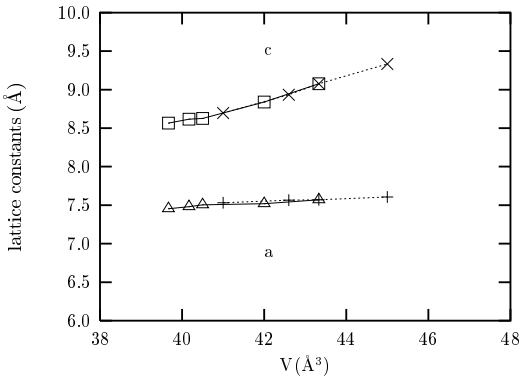

Figure 19. The variations of the lattice constants of keatite with volume. Full curves, triangles and squares: LDA; broken curves and crosses: GGA.

3.5. Coesite

Coesite is a high-pressure polymorph of silica with a rather complex monoclinic structure. The space-group symmetry has been described as $C2/c$ by Smyth *et al* [51] and Geisinger *et al* [100]

and as $P2_1/c$ by Kirfe *et al* [101]. Because of the properties of the lattice constants ($a \approx c$ and $\beta \approx 120^\circ$), the symmetry can also be characterized as pseudohexagonal. Within the $P2_1/c$ setting, the unit cell contains 16 SiO_2 units. All Si and O atoms occupy Wyckoff positions (4e) with three independent internal parameters. Hence at fixed volume a complete optimization of the structure requires the minimization of the total energy with respect to 40 independent parameters. In the $C2/c$ structure Si1 and Si2 atoms occupy Wyckoff positions (8f) with coordinates (u, v, w), O1 atoms occupy positions (4a) with coordinates $(0, 0, 0)$, O2 atoms occupy positions (4e) with coordinates $(\frac{1}{2}, y, \frac{3}{4})$ and O3 to O5 atoms occupy positions (8f) with three independent positional parameters. Because of the higher symmetry, only a total-energy minimization with respect to 20 independent parameters is required. A projection of the $P2_1/c$ structure is shown in figure 20. The connectivity of the network of SiO_4 tetrahedra is very similar in the $C2/c$ variant. In coesite the SiO_4 tetrahedra form two kinds of four-membered ring; one is approximately parallel to (101), the other to (110). The calculations have been performed on a $3 \times 3 \times 3$ $\vec{k}$-point grid corresponding to ten irreducible points (for both structures).

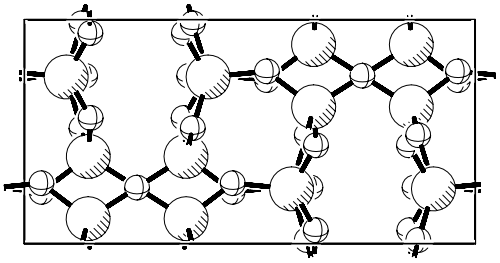

Figure 20. A representation of the crystal structure of coesite (space-group symmetry $P2_1/c$).

The results of the structural optimizations are given in table 8 for $C2/c$ and table 9 for $P2_1/c$. For the more symmetric $C2/c$ lattice the LDA underestimates the equilibrium volume by about 2.4%, whereas the GGA leads to a 3% overestimate. The lattice parameters and monoclinic angle are predicted with comparable accuracy. The difference between the shortest and the longest Si–O distances calculated within the LDA agrees within ≈0.015 Å with the experimentally observed difference, whereas the larger equilibrium volume of the GGA allows for a smaller difference with a maximum of ≈0.01 Å. The distortions of the intra-tetrahedral angles are small, but it is remarkable that even these small variations are predicted with good accuracy. Because of the centrosymmetric position of the O1 atoms, the Si1–O1–Si1 bonds are aligned, whereas the other Si–O–Si bond angles vary between 136.5° and 149.6°—again it is remarkable that within the LDA all angles are correct within a maximum error of 0.7°.

For the $P2_1/c$ structure the LDA predicts the equilibrium volume with an accuracy of 1%, whereas the GGA leads to an overestimate of about 4.5%. The predictions of the axial ratios and of the monoclinic angle are of comparable accuracy. Because of the low symmetry, there are 16 non-equivalent Si–O distances varying between 1.581 Å and 1.614 Å (LDA), in good agreement with the experimentally determined distances spreading between 1.583 Å and 1.621 Å (except the Si2–O3 and Si3–O4 distances). The intra-tetrahedral angles vary between 107.7° and 110.5° (LDA) and between 105.9° and 111.7° (experiment), respectively. There are eight inter-tetrahedral Si–O–Si bond angles varying between 137.0° and 149.7° (LDA) and between 136.4° and 150.2° (experiment) and a Si1–O7–Si2 bond angle close to 180°. All inter-tetrahedral angles increase on expansion, with the Si3–O8–Si4 angle showing the strongest variation. This angle describes the concatenation of the SiO_4 tetrahedra parallel to the c-axis

Table 8. Structural parameters, bond lengths (in Å), bond angles (in degreees), cohesive energies and bulk moduli for coesite ($C2/c$).

	Experiment[a]	GGA	LDA
a (Å)	7.1357	7.2419	7.0672
b (Å)	12.3835	12.467	12.2907
c (Å)	7.1859	7.2327	7.14057
c/a	1.0070	0.9987	1.01037
c/b	0.5802	0.5801	0.5809
β (deg)	120.375	120.169	120.416
V/SiO_2 (Å^3)	34.23	35.28	33.43
Si1(u, v, w)	0.1399, 0.1084, 0.0721	0.1428, 0.1072, 0.0736	0.1386, 0.1087, 0.0719
Si2(u, v, w)	0.5072, 0.1578, 0.5415	0.5073, 0.1580, 0.5402	0.5069, 0.1574, 0.5419
O1(x, y, z)	0.0, 0.0, 0.0	0.0, 0.0, 0.0	0.0, 0.0, 0.0
O2(x, y, z)	0.5, 0.1152, 0.75	0.5, 0.1175, 0.75	0.5, 0.1140, 0.75
O3(x, y, z)	0.2640, 0.1245, 0.9383	0.2710, 0.1195, 0.9441	0.2628, 0.1256, 0.9378
O4(x, y, z)	0.3127, 0.1031, 0.3276	0.3101, 0.1057, 0.3289	0.3132, 0.1029, 0.3272
O5(x, y, z)	0.0190, 0.2117, 0.4766	0.0106, 0.2117, 0.4781	0.0203, 0.2119, 0.4745
Si1–O1	1.5960	1.6085	1.5818
Si1–O3	1.6149	1.6239	1.6068
Si1–O4	1.6147	1.6215	1.6043
Si1–O5	1.6262	1.6293	1.6137
Si2–O2	1.6135	1.6245	1.6026
Si2–O3	1.6178	1.6238	1.6069
Si2–O4	1.6089	1.6150	1.5953
Si2–O5	1.6229	1.6284	1.6139
O1–Si1–O3	110.59	110.3	110.5
O1–Si1–O4	109.14	110.8	109.0
O1–Si1–O5	109.77	109.7	110.2
O3–Si1–O4	110.43	110.0	110.2
O3–Si1–O5	107.91	108.3	108.0
O4–Si1–O5	108.98	107.7	108.9
O2–Si2–O3	109.75	109.8	109.9
O2–Si2–O4	109.4	109.3	109.7
O2–Si2–O5	110.09	110.3	109.9
O3–Si2–O4	108.79	108.6	108.8
O3–Si2–O5	109.33	109.6	109.0
O4–Si2–O5	109.45	109.2	109.5
Si1–O1–Si1	180	180	180
Si2–O2–Si2	141.81	143.8	141.1
Si1–O3–Si2	144.11	145.1	144.2
Si1–O4–Si2	149.66	150.7	149.9
Si1–O5–Si2	136.54	139.6	136.2
E_0 (eV/SiO_2)		−23.7318	−25.9522
B_0 (GPa)		91.2	94.3
B_0'		4.5	4.8

[a] Reference [51].

whereas the other angles characterize the angles in the four-membered rings of tetrahedra (see also figure 20).

One of the characteristic properties of coesite is the strong anisotropy of the pressure-induced contraction of the lattice constants and the strong anisotropy of the thermal expansion.

Table 9. Structural parameters, bond lengths (in Å), bond angles (in degrees), cohesive energies and bulk moduli for coesite ($P2_1/c$).

	Experiment[a]	GGA	LDA
a (Å)	7.098, 7.135, 7.1367	7.235	7.076
b (Å)	12.334, 12.383, 12.3695	12.485	12.297
c (Å)	7.148, 7.185, 7.1742	7.241	7.137
c/a	1.007, 1.007, 1.005	1.000	1.008
c/b	0.579, 0.580, 0.5799	0.5804	.5804
β (deg)	120.10, 120.37, 120.34	120.19	120.29
V/SiO_2 (Å^3)	33.83, 34.23	35.34	33.52
Si1(u, v, w)	0.6090, 0.3585, 0.9314	0.6077, 0.3572, 0.9273	0.6107, 0.3583, 0.9293
Si2(u, v, w)	0.8894, 0.3582, 0.5758	0.8926, 0.3572, 0.5744	0.8887, 0.3585, 0.5731
Si3(u, v, w)	0.2568, 0.4086, 0.0442	0.2566, 0.4082, 0.0399	0.2559, 0.4074, 0.0419
Si4(u, v, w)	0.2438, 0.4074, 0.4628	0.2438, 0.4080, 0.4613	0.2443, 0.4073, 0.4605
O1(x, y, z)	0.4391, 0.3548, 0.6742	0.4413, 0.3546, 0.6717	0.4388, 0.3530, 0.6738
O2(x, y, z)	0.4856, 0.3726, 0.0647	0.4781, 0.3694, 0.0551	0.4843, 0.3735, 0.0614
O3(x, y, z)	0.7319, 0.4648, 0.5184	0.7390, 0.4619, 0.5200	0.7302, 0.4621, 0.5216
O4(x, y, z)	0.7666, 0.4581, 0.9749	0.7614, 0.4618, 0.9803	0.7689, 0.4619, 0.9780
O5(x, y, z)	0.0184, 0.3738, 0.4459	0.0228, 0.3690, 0.4471	0.0161, 0.3735, 0.4416
O6(x, y, z)	0.0597, 0.3530, 0.8297	0.0596, 0.3546, 0.8296	0.0598, 0.3537, 0.8288
O7(x, y, z)	0.7514, 0.2515, 0.0012	0.7498, 0.2499, 0.002	0.7497, 0.2498, 0.0020
O8(x, y, z)	0.2480, 0.3662, 0.2519	0.2505, 0.3697, 0.2507	0.2508, 0.3654, 0.2515
Si1–O1	1.6168	1.6231	1.6039
Si1–O2	1.5945	1.6222	1.6040
Si1–O4	1.5840	1.6308	1.6142
Si1–O7	1.5835	1.6081	1.5812
Si2–O3	1.6394	1.6302	1.6124
Si2–O5	1.6095	1.6228	1.6064
Si2–O6	1.6000	1.6221	1.6036
Si2–O7	1.5974	1.6088	1.5814
Si3–O2	1.6179	1.6238	1.6063
Si3–O4	1.6517	1.6289	1.6136
Si3–O6	1.6212	1.6170	1.5956
Si3–O8	1.6048	1.6219	1.6004
Si4–O1	1.5894	1.6178	1.5952
Si4–O3	1.5844	1.6286	1.6127
Si4–O5	1.5976	1.6240	1.6057
Si4–O8	1.6055	1.6221	1.6013
Si1–O1–Si4	150.2	149.7	149.6
Si1–O2–Si3	143.4	145.4	144.5
Si2–O3–Si4	138.2	139.9	137.0
Si1–O4–Si3	136.4	139.6	137.2
Si4–O5–Si2	145.6	145.7	144.8
Si2–O3–Si3	149.2	149.7	149.7
Si3–O8–Si4	142.5	145.7	142.4
Si1–O7–Si2	177.7	179.3	179.6
E_0 (eV/SiO_2)		−23.7327	−25.9521
B_0 (GPa)		88.3	92.6
B_0'		5.6	4.26

[a] Reference [6].

Increasing the pressure from 0 to 5.2 GPa leads to a contraction of a by 2%, whereas b and c change only by 1.1% and 0.9% respectively (reference [102]). Indeed, figure 21 demonstrates that in the $C2/c$ structure a depends more strongly on the cell volume than b and c, the monoclinic angle remaining almost constant. A similar anisotropy is predicted for the $P2_1/c$ structure. Within the LDA, the total energies of the two structural variants agree to within 0.1 meV/SiO_2 unit; in the GGA the $P2_1/c$ structure is lower in energy by 0.9 meV/SiO_2. Both values are at, or even below, the limit of accuracy of our calculation, so the conclusion is that the two structures are essentially energetically degenerate. The calculated bulk modulus is more than twice as large as that for α-quartz and only 30% lower than that of β-quartz. The bulk modulus calculated for the $P2_1/c$ structure is slightly lower, in accordance with the expectation based on the lower symmetry

Unlike for the low-density polymorphs, the gradient corrections have a pronounced influence on the structural energy differences of coesite. Within the LDA we calculate a difference of $\Delta E = 0.011$ eV/SiO_2 unit relative to the energy of α-quartz whereas the gradient corrections lead to a nearly nine times larger value of $\Delta E = 0.094$ eV/SiO_2 unit, which can be compared to the experimental enthalpy difference extrapolated to 0 K, $\Delta H = 0.05$ eV [47]. Hence the gradient corrections will have a strong influence on the

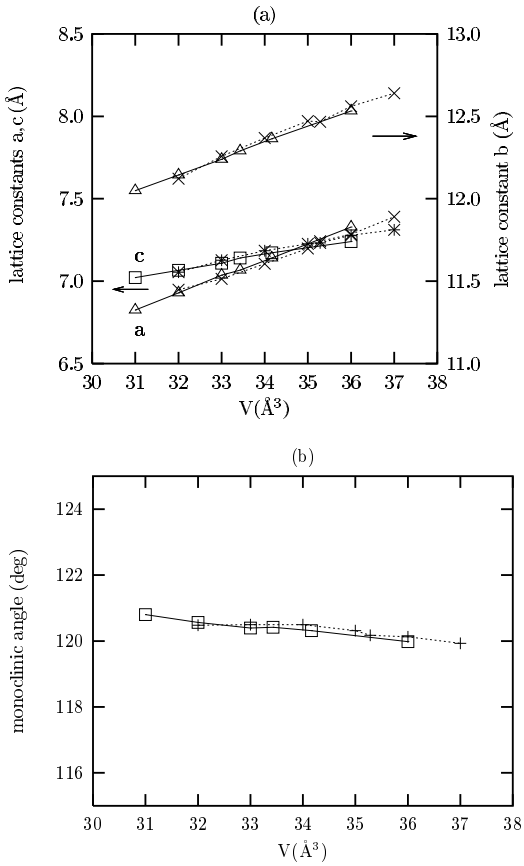

Figure 21. The variations of the lattice parameters a, b and c (a) and of the monoclinic angle β (b) of coesite ($C2/c$) with volume. Full curves, triangles and squares: LDA; broken curves, crosses and stars: GGA.

energetics of the pressure-induced phase transitions. We shall come back to this point in connection with the coesite/stishovite and quartz/stishovite phase transitions.

3.6. Stishovite

Stishovite was first synthesized in the laboratory [7] and later discovered in meteor craters. Stishovite is isostructural with rutile (TiO_2). The space group is $P4_2/mnm$; the unit cell contains two SiO_2 units. Si occupies the octahedral (2a) positions with coordinates $(0, 0, 0)$ and $(1/2, 1/2, 1/2)$, O the positions (4f) with coordinates $(x, x, 0)$. Each Si atom is octahedrally coordinated by six O atoms; each O atom is coordinated by three Si atoms. A graphical representation of the structure of stishovite along the *b*-axes is given in figure 22. The chemical bonding is expected to be fundamentally different from that in the tetrahedrally coordinated low-pressure phases where each Si is surrounded by four O and each O by two Si only. As a consequence of the different coordinations, the Si–Si and O–O distances decrease at the pressure-induced transformation from coesite to stishovite, but the Si–O distances increase substantially. Therefore the stiffness of the Si–O bonds is the driving factor behind the change from tetrahedral to octahedral coordination.

For a structural optimization at constant volume, only two independent parameters remain to be determined. Our calculations have been performed using a $4 \times 4 \times 4$ $\vec{k}$-point mesh,

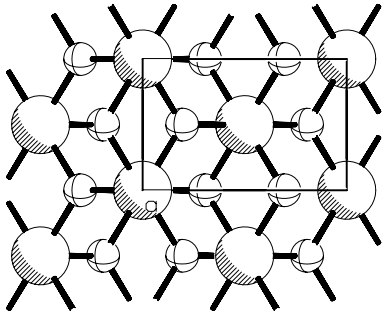

Figure 22. A representation of the crystal structure of stishovite (space-group symmetry $P4_2/mnm$).

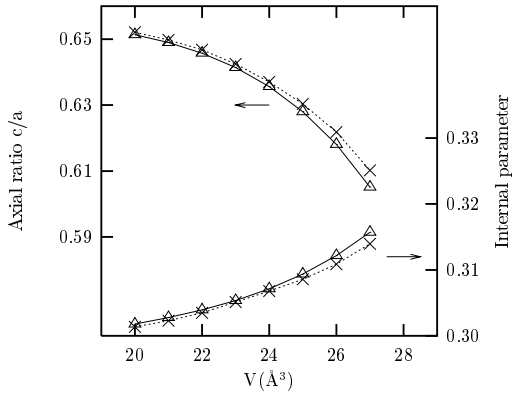

Figure 23. The variations of the axial ratio c/a and of the internal parameter x of the stishovite structure with volume. Full curves and triangles: LDA; broken curves and crosses: GGA.

Table 10. Structural parameters, bond lengths (in Å), bond angles (in degrees), cohesive energies and bulk moduli for stishovite ($P4_2/mnm$).

	Experiment[a]	GGA	LDA	GGA[b]	LDA[b]	HF[c]	LAPW[d]
a (Å)	4.179, 4.18	4.2387	4.1636	4.29	4.20	4.15	4.16
c (Å)	2.666, 2.667	2.7005	2.6696	2.68	2.65	2.69	2.66
c/a	0.6380, 0.6382	0.6371	0.6411	0.6247	0.6309	0.6481	0.640
V/SiO_2 (Å^3)	23.3, 23.31	24.26	23.14	24.66	23.37	23.16	23.01
O(x)	0.3061, 0.3067	0.3071	0.3056	0.292	0.296	0.306	0.306
Si–O	1.76	1.7775	1.7584	1.77	1.76		1.75
Si–O	1.81	1.8412	1.7994	1.87	1.82		1.80
Si–O–Si	130.6	130.6	130.6	132.5	131.7		130.6
E_0 (eV/SiO_2)		−23.1894	−25.8596				
B_0 (GPa)	313	261	293	260	286		324
B_0'	2.8–6	2.8	4.1	3.0	4.6		4.0

[a] References [103, 104].
[b] Reference [29].
[c] Reference [46].
[d] Reference [37].

corresponding to six irreducible special points. Our results are compiled in table 10. The LDA predicts the equilibrium volume with an accuracy of 0.7%, whereas the GGA overestimates the volume by 4.2%. Within this small volume change there is almost no variation of the structural parameters—hence the agreement with experiment (references [103, 104]) is equally good in both approximations. Over a wider range of volumes, we find an appreciable decrease of the axial ratio on expansion, accompanied by an increase of the internal parameter x (see figure 23). At fixed volume there is no difference at all between the LDA and GGA predictions. The theoretical predictions are well confirmed by experiment (references [103, 104]) over a limited range of pressures. In terms of the local structure, the change of the axial ratio and internal parameter is reflected in an increasing difference in the Si–O1 and Si–O2 distances on expansion while the Si–O–Si bond angle remains almost unchanged (see figure 24). This shows

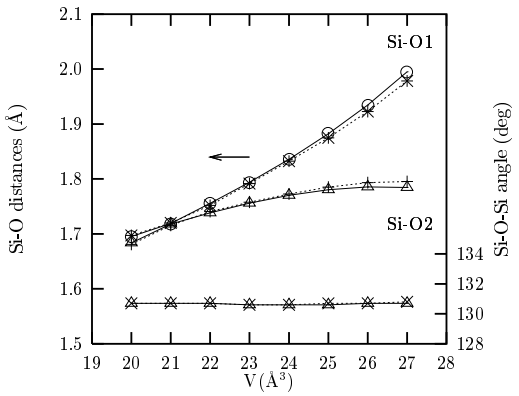

Figure 24. The variations of the Si–O1 and Si–O2 distances and of the Si–O–Si bond angle in stishovite as functions of volume. Full curves, triangles and circles represent LDA results; broken curves and crosses represent GGA results.

that at zero pressure the apical bonds in the octahedron are longer than the equatorial bonds. On expansion the octahedron is elongated; on compression the apical bonds eventually become even shorter than the equatorial bonds. The calculated LDA equation of state is in excellent agreement with the available experimental data (figure 25). The predicted bulk modulus is also in good agreement with experiment, while the experimental values for its pressure derivative scatter too much to allow any conclusion to be reached. We note that the bulk modulus of stishovite is larger than those of all other oxides with the rutile structure and also larger than those of any known silicates.

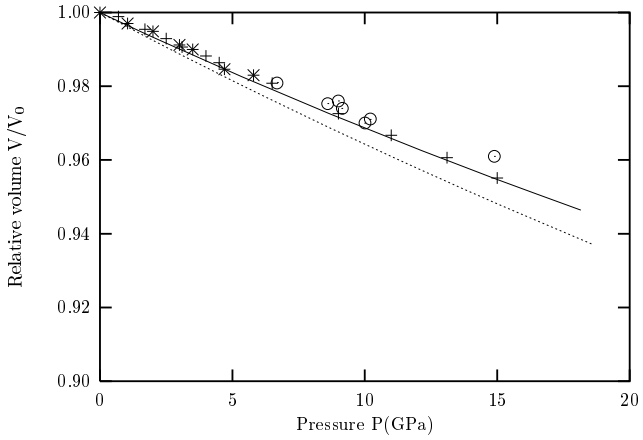

Figure 25. The equation of state of stishovite. The full curve represents LDA results; the broken curve represents GGA results. The experimental data are from Liu *et al* (reference [109], circles), Sugiyama *et al* (reference [103], stars) and Ross *et al* (reference [104], crosses).

Because of the simplicity of its crystal structure, a number of *ab initio* calculations of the structural and cohesive properties of stishovite have been performed. Park *et al* [36] and Cohen [37] used the all-electron LAPW method, based on the LDA. A number of pseudopotential-based LDA calculations have been performed by different groups [29–33]. Hamann [29] investigated also the influence of generalized-gradient corrections. The good agreement of the all-electron calculations of Cohen [37] with the present LDA results confirms that our ultrasoft pseudopotentials are accurate and transferable; the agreement of both his LAPW and our pseudopotential calculations with the Hartree–Fock calculations of Sherman [46] shows that the LDA should in principle be adequate. Concerning the influence of gradient corrections, our results are in essential agreement with those of Hamann [29]. The pseudopotential-based calculations are in reasonable agreement with the present work. The error in the equilibrium volume is in the range $\Delta V = -0.05$ to 0.23 Å^3 per SiO_2 unit, except for the results of Keskar and Chelikowsky [31] predicting a somewhat smaller equilibrium volume ($\Delta V = -0.32$ Å^3/SiO_2).

An important result is, as already emphasized by Hamann [29], that the GGA predicts a much larger structural energy difference between α-quartz and stishovite than the LDA: ΔE(LDA) = 0.1044 eV/SiO_2 unit, ΔE(GGA) = 0.6367 eV/SiO_2 unit. To check the influence of the precise form of the gradient corrections, the calculations for α-quartz and stishovite have been repeated with the Perdew–Becke (PB) [55, 56] functional. The PB functional leads to even stronger corrections to the LDA: the equilibrium volumes of α-quartz and stishovite increase by 0.84 Å^3/SiO_2 and 0.31 Å^3/SiO_2 relative to the functional of Perdew *et al* (reference [25]); the structural energy difference increases to $\Delta E = 0.691$ eV/SiO_2

unit. Hamann reports quartz–stishovite energy differences of $\Delta E = 0.02$ eV/SiO_2 (LDA) and $\Delta E = 0.57$ eV/SiO_2 (GGA); other LDA results include $\Delta E = 0.07$ eV/SiO_2 (Liu *et al*, reference [32]) and $\Delta E = 0.086$ eV/SiO_2 (Keskar and Chelikowsky, reference [31]). A Hartree–Fock calculation by Sherman [46] yields $\Delta E = 0.57$ eV/SiO_2, to be compared with the experimental estimate of Holm *et al* [47] $\Delta E \approx 0.53$ eV/SiO_2 and the experimental enthalpy differences at 298 K of 0.51 eV (reference [47]) and of 0.54 eV (reference [48]).

3.7. Pressure-induced phase transitions

Given the structural energy differences and the energy/volume and pressure/volume relations of the competing phases, the critical pressures for pressure-induced phase transitions may be determined by equating the free enthalpies (or the enthalpies in the limit of zero temperature) and the pressures. In an energy/volume diagram this is equivalent to constructing the common tangent to two $E(V)$ curves. Table 11 summarizes the structural energy differences calculated in the LDA and GGA, figures 26 and 27 the energy–volume relations and figure 28 the enthalpy–pressure relations for α-quartz, stishovite and coesite.

In the LDA, α-quartz has the lowest total energy; pressure-induced phase transitions at low temperature to the denser coesite and stishovite phases are possible; all other polymorphs can

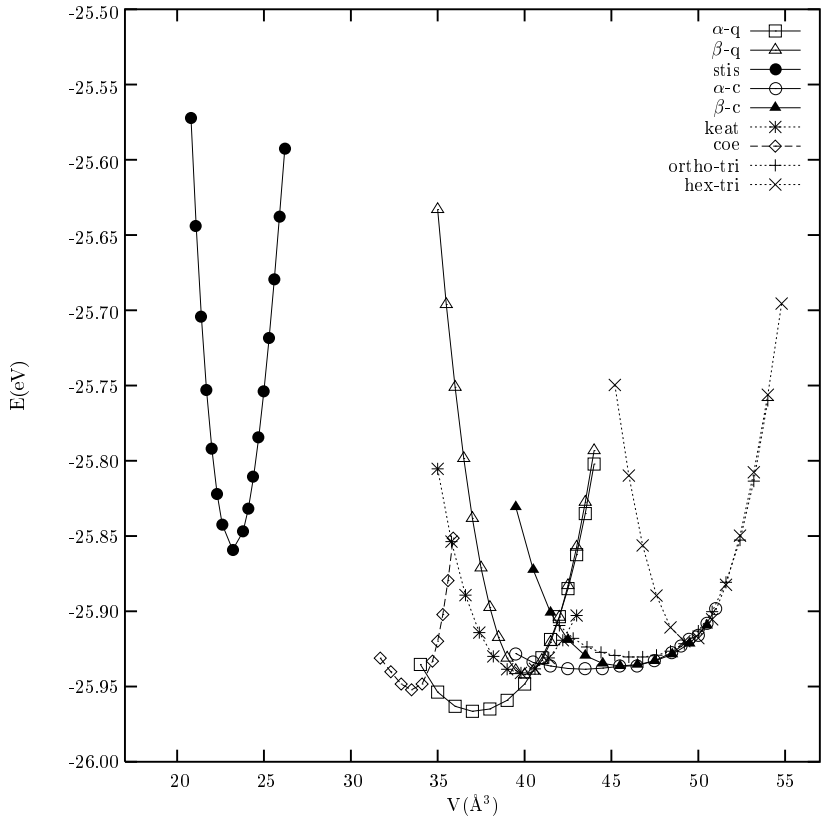

Figure 26. Energy versus volume curves for the silica polytypes, calculated in the LDA. For β-cristobalite only the result for the energetically most favourable structural variant ($I\bar{4}2d$) is shown.

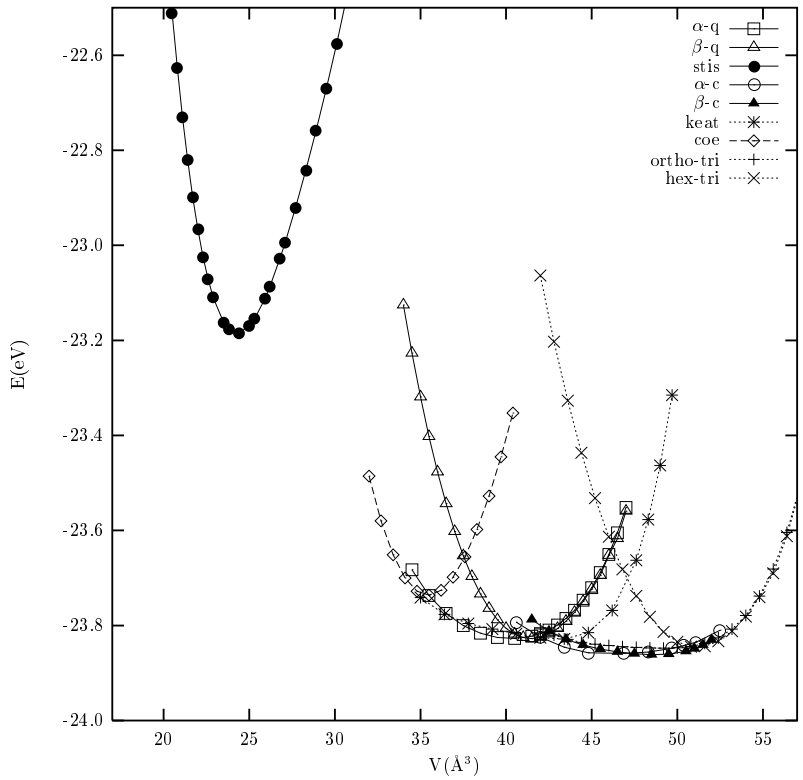

Figure 27. As figure 26, but calculated in the GGA. Note the change in energy scale relative to figure 26.

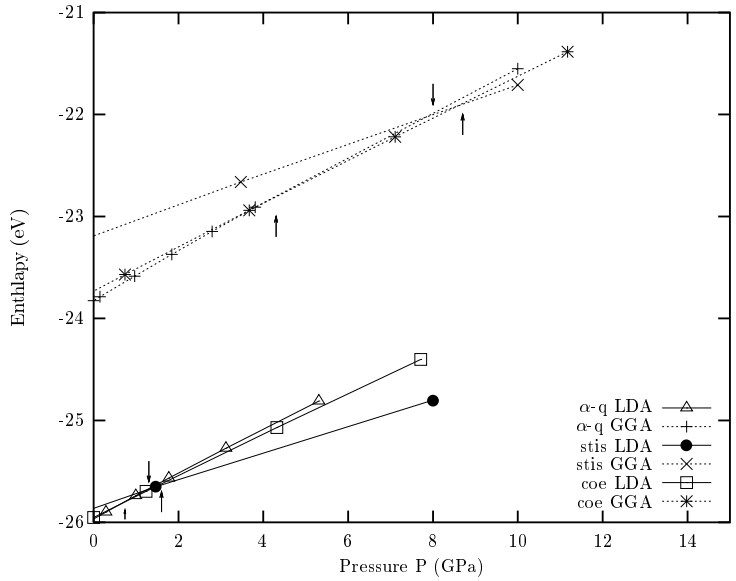

Figure 28. Enthalpy–pressure relations for α-quartz, coesite and stishovite calculated in the LDA and the GGA. The vertical arrows mark the transition pressures.

Table 11. Calculated structural energy differences in eV/SiO_2 between the silica polymorphs. Upper right: LDA; lower left: GGA.

					Quartz		Cristobalite		
		Stishovite	Keatite	Coesite	α	β	α	β	Tridymite
					LDA				
Stishovite		0	−0.0820	−0.0926	−0.1044	−0.0785	−0.0791	−0.0778	−0.0706
Keatite		−0.6387	0	−0.0105	−0.0224	0.0035	0.0028	0.0041	0.0114
Coesite	G	−0.5424	0.0963	0	−0.0118	0.0140	0.0134	0.0147	0.0219
α-quartz	G	−0.6367	0.0020	−0.0943	0	0.0259	0.0252	0.0265	0.0338
β-quartz	A	−0.6347	0.0040	−0.0923	0.0019	0	−0.0006	0.0006	0.0079
α-cristobalite		−0.6685	−0.0297	−0.1260	−0.0317	−0.0337	0	0.0012	0.0085
β-cristobalite		−0.6741	−0.0354	−0.1317	−0.0374	−0.0394	−0.0056	0	0.0072
Tridymite		−0.6591	−0.0203	−0.1166	−0.0223	−0.0243	0.0094	0.0150	0

be obtained only at expanded volume at higher temperatures. For the α-quartz $\rightarrow$ coesite phase transition we calculate a critical pressure of $p_c(\alpha\text{-coesite}) \sim 0.74$ GPa, i.e. a factor of two lower than that corresponding to the extrapolation of the coexistence line in the phase diagram to zero temperature. The discrepancy is similar for the metastable α-quartz $\rightarrow$ stishovite transition and to the coesite $\rightarrow$ stishovite transition (see table 11). The larger structural energy differences predicted by the GGA improve substantially on the theoretical estimates for the transition pressures of the α-quartz $\rightarrow$ stishovite and coesite $\rightarrow$ stishovite transitions which are now in better agreement with experiment (see table 12). Concerning the GGA prediction for the α-quartz $\rightarrow$ stishovite transition we note a good agreement with the calculation of Hamann [29]. For the α-quartz $\rightarrow$ coesite transitions, however, the GGA corrections overshoot: the critical pressure is now too high by a factor of almost 2.4. Thus the conclusion is that the much larger structural energy differences between α-quartz and the high-pressure polymorphs resulting from the GGA are for stishovite much more realistic than the LDA predictions, but for coesite the discrepancy is about the same in the LDA and in the GGA. However, we must also remember that the GGA leads to lower values for the bulk modulus and also to lower pressures than the LDA (which, in this respect, leads to better agreement with experiment). Hence the structural energy differences resulting from the GGA are probably somewhat too large (cf. also the comparison with the experimental estimates for the α-quartz $\rightarrow$ stishovite ΔE given in the last section), but this error is compensated by a less accurate (softer) equation of state.

Table 12. Calculated equilibrium pressures for structural phase transitions (in GPa).

	LDA	GGA	Experiment
α-quartz $\rightarrow$ coesite	0.74	4.3	1.8[b]
α-quartz $\rightarrow$ stishovite	1.3	8.0	7.2[a]
Coesite $\rightarrow$ stishovite	1.6	8.7	7.2[b]

[a] Reference [48].
[b] Extrapolated from the coexistence line in the phase diagram of reference [2].

The situation is less clear for the low-density polymorphs. Within the LDA, the modifications of α-cristobalite and keatite are higher in energy than β-quartz. Hence at zero temperature the corresponding coexistence lines in the phase diagram should extrapolate to a negative pressure of ~ -0.6 GPa estimated from the common-tangent constructions, in reasonable agreement with the experimental phase diagram. Within the GGA, α- and β-quartz

are energetically almost degenerate, the two cristobalite phases are lower in energy by about 0.03 eV/SiO_2 and even tridymite is predicted to be lower in energy by ∼0.02 eV/SiO_2. Hence the phase coexistence lines would be expected to extrapolate to small positive pressures, with β-cristobalite being the stable ($p = 0, T = 0$) polymorph. Since α-cristobalite is also much softer than α-quartz, it is not to be expected that the relative stabilities resulting from the static total-energy calculations could be reversed by the differences in the zero-point vibrational energies.

In summary we find that the GGA leads to a more realistic description of the high-density polymorphs, but reverses the order of stability of the low-density polytypes.

4. Discussion and conclusions

We have presented detailed calculations of the structural properties and energetics of silica in the 'low'- and 'high'-quartz, 'low'- and 'high'-cristobalite, tridymite, keatite, coesite and stishovite structures within the local density and generalized-gradient approximations. Our calculations are based on highly accurate pseudopotentials and rigorous convergence criteria. We have demonstrated that we are able to reproduce the structural properties of even the most complex known silica polymorphs with high accuracy. Our calculated equations of state agree with experiment essentially within experimental uncertainty; the analysis of the variations of the crystal structures with the unit-cell volume leads to interesting insights into the mechanism of the structural phase transitions. For the transition between the 'low'- and 'high'-phases of quartz, our calculations demonstrate the possibility of a continuous phase transition. We have also studied different structural variants proposed for 'high'-cristobalite and 'high'-tridymite. The fact that for cristobalite we find all proposed structures energetically almost degenerate over a rather wide range of densities lends credit to the suggestions [85, 96] that the different variants reported in the literature are due to different sample treatments. We have also studied the possibilities of transitions between the different structural variants. We find that the presence of the simple cubic and tetragonal variants of β-cristobalite considerably complicates the scenario for the $\alpha \rightarrow \beta$ transition—while there is a possibility of a continuous transition from the α- to the 'ideal' β-phase with the $Fd3m$ symmetry, the transition to the low-symmetry β-variants being necessarily first order. Similarly, for tridymite our results indicate that the $P6_3/mmc$ symmetry is an idealization of the true tridymite structure, in the same way as in the case for the ideal cristobalite structure. The orthorhombic phase of tridymite is shown to undergo a continuous transition to the hexagonal structure on expansion. For keatite we find that the proposed structure is energetically competitive in the density range between quartz and cristobalite.

Our calculations provide a complete set of bulk moduli for the tetrahedrally coordinated phases of SiO_2. Our results demonstrate that there is a clear connection between the value of the bulk modulus and the flexibility of the network of the SiO_4 tetrahedra. For β-quartz and the idealized structures of β-cristobalite ($Fd3m$) and 'high'-tridymite ($P6_3/mmc$), where there is no flexibility in the lattice (no 'soft coordinate'), B_0 is of the order of 130–140 GPa. For α-quartz and the tetragonal ($I\bar{4}2d$) version of β-cristobalite, where there is one 'soft coordinate' connected with a rigid rotation of the SiO_4 tetrahedra, the bulk modulus is about 28 to 35 GPa. With three 'soft coordinates' like in α-cristobalite, B_0 is of the order of 12 GPa. The intermediate values of $B_0 \sim 94$ GPa for coesite and $B_0 \sim 52$ GPa for keatite indicate that although there is formally no soft coordinate, some degrees of freedom have a reduced elastic energy. The details of this structure property relationship remain to be explored.

Our results show that at fixed volume the local density and generalized-gradient approximations lead to absolutely identical structural predictions, confirming the similar

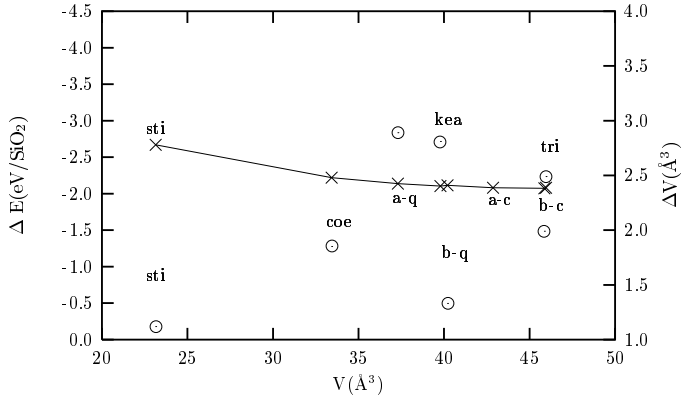

Figure 29. GGA corrections to the total energy (ΔE, crosses and left-hand scale) and to the equilibrium volume (ΔV, circles and right-hand scale) of the silica polytypes. The solid curve is a guide to the eye emphasizing the trend in the total-energy corrections.

observations made on the crystal structures of the elements from groups IV to VI of the Periodic Table [20, 28]. The GGA makes an isotropic contribution to the internal pressure, favouring expansion. This effect is stronger in the more open structures: in stishovite the gradient corrections expand the volume by 4.2%, in α-quartz they expand it by 6.6% and in α-cristobalite they expand it by 9.8% (see figure 29). While, with the exception of that for tridymite, the LDA predictions for the equilibrium volume are accurate within $\pm 2\%$, the GGA error varies between 4.2% (stishovite) and 9.8% (α-cristobalite). The GGA is also consistently less accurate for the equation of state, the bulk modulus and, by an indirect effect, for the structural properties.

The gradient corrections are, however, essential for predicting the pressure-induced phase transitions: in the LDA the structural energy differences between α-quartz, coesite and stishovite are seriously underestimated and this leads to transition pressures much lower than in experiment. Figure 29 summarizes the GGA corrections to the equilibrium volume and total energy. We find that the corrections both to the total energy and to the volume increase with decreasing density of the silica polymorphs. We have plotted the differences in the total energies. These are always smaller than the gradient corrections to the total energies of the free atoms (for reference, ΔE(LDA–GGA) $= -3.33$ eV for one Si and two O atoms together). Hence for the cohesive energy the GGA leads to a reduction which is smaller for the low-density than for the high-density polymorphs. In contrast to the smooth variation of ΔE(LDA–GGA) with density, the gradient corrections to the equilibrium volume depend strongly on symmetry constraints: ΔV(LDA–GGA) is substantially larger for 'low'-quartz and 'low'-cristobalite than for the corresponding high-temperature polytypes. The reason for this is that the stretching of the Si–O–Si bonds in the low-symmetry phases resulting from an increase of the internal pressure leads to a stronger expansion.

Although the GGA improves the description of the pressure-induced phase transitions to the high-density polytypes, it destroys the correct order of stability among the low-density polytypes: cristobalite, keatite and even tridymite are now predicted to be energetically more favourable than quartz, in disagreement with the shapes of the coexistence lines in the phase diagram. Hence we cannot agree with Hamann's conclusion that the fact that the pressure-induced quartz–stishovite transition is better described in the GGA reflects the fact that the GGA would be capable of a more accurate treatment of the exchange–correlation energy density in

regions of exponential charge decay. The fact that the GGA corrections are *isotropic* is caused by the fact that the largest contributions to the gradient corrections stem from regions close to the ionic core, as concluded by Juan and Kaxiras [105] on the basis of an investigation of the local variations in the exchange–correlation energy density induced by the gradient corrections. In more compact crystal structures the large density gradients are partially levelled out by overlaps from neighbouring atoms; therefore gradient corrections tend to be smaller.

Altogether, the conclusions concerning the role of gradient corrections remains unsatisfactory: the GGA improves on the structural energy differences between structures with widely different local connectivities, but leads to poorer results for structural, cohesive and elastic properties. Preliminary results show that the LDA also gives good agreement for the phonon spectrum of α-quartz (reference [106]).

Our results should also be seen in the context of recent work on the denser post-stishovite phases [38] and on porous forms of silica and aluminosilicates. The recent work of Teter *et al* [38], also based on the VASP and the LDA, demonstrates the possibility of extensive polymorphism of silica at very high pressure, with an infinite number of structures describable as eutectic hexagonal close-packed arrays of oxygen with half of the octahedral interstices filled in different ways by silicon. A post-stishovite sequence of stable phases, stishovite $\rightarrow$ $CaCl_2$-type $\rightarrow$ α-PbO_2-type $\rightarrow$ Pa3-type, has been proposed [38]. On the other hand, first *ab initio* calculations of porous aluminosilicates (zeolites), including the purely siliceous forms of these materials, are becoming available (references [107,108]). These calculations include structures as complex as mordenite with 48 SiO_2 units per cell in the purely siliceous form.

Finally, we would like to mention that very recent work on polymorphism in zirconia (reference [110]) leads to very similar conclusions: the LDA yields consistently more accurate predictions of the structures of all polytypes, but the structural energy differences between phases with different Zr–O coordinations are quantitatively correct only if gradient corrections are used. Hence we can conclude that the LDA allows one to determine the crystal structures of even complex inorganic compounds with high accuracy. To predict the energetics of the competing phases with an accuracy sufficient to give quantitatively accurate results for transition pressures without causing deterioration in the high quality of the calculated structures and predicting accurate equations of state requires the construction of an improved gradient functional.

Acknowledgments

This work was performed within the Groupement de Recherche Européen (GdR-E) 'Dynamique moléculaire quantique appliquée à la Catalyse, à l'Adsorption et à l'Absorption', supported by the Centre National de la Recherche Scientifique (CNRS) and the Institut Français du Pétrole (IFP). The Nancy–Vienna cooperation was supported within the framework of the bilateral Austro-French Agreement on Scientific Cooperation (Amadeus). Fruitful discussions with Professor B Silvi are gratefully acknowledged. The authors are also indebted to A L Speck for providing us with his package PLATON which was used to generate the silica pictures in this article.

References

[1] Bragg L and Claringbull G F 1965 *Crystal Structures of Minerals* (London: Bell)

[2] Hemley R J, Prewitt C T and Kingma K J 1994 *Silica: Physical Behaviour, Geochemistry and Materials Applications (Reviews in Mineralogy vol 29)* (Washington, DC: Mineralogical Society of America)

[3] Wyckoff R W G 1965 *Crystal Structures* 2nd edn (New York: Wiley–Interscience)

[4] Sosman R B 1965 *The Phases of Silica* (New Brunswick, NJ: Rutgers University Press)
[5] Merill L 1988 *J. Phys. Chem. Ref. Data* **334** 52
[6] Villars P and Calvert N 1993 *Pearsons's Handbook of Crystallographic Data* 2nd edn (Metals Park, OH: American Society for Metals)
[7] Stishov S M and Popova S V 1961 *Geokhimiya* **10** 873
[8] Kingma K J, Cohen R E, Hemley R J and Mao H K 1995 *Nature* **374** 243
[9] Karki B B, Warren M C, Stixrude L, Ackland G J and Crain J 1997 *Phys. Rev.* B **55** 3465
[10] Belonoshko A B, Dubrovinsky L S and Dubrovinsky N A 1996 *Am. Mineral.* **81** 785
[11] Tse J S, Klug D D and LePage Y 1992 *Phys. Rev. Lett.* **69** 3647
Tse J S, Klug D D and Allan D C 1995 *Phys. Rev.* B **51** 16 392
[12] Catlow C R A and Price G D 1990 *Nature* **347** 243
[13] Boisen M B and Gibbs G V 1993 *Phys. Chem. Minerals* **20** 123
Boisen M B, Gibbs G V and Bukowinski M S T 1994 *Phys. Chem. Minerals* **21** 269
[14] Car R and Parrinello M 1985 *Phys. Rev. Lett.* **55** 2656
[15] Payne M C, Teter M P, Allan D C, Arias T A and Joannopoulos J D 1992 *Rev. Mod. Phys.* **64** 1045
[16] Kresse G and Hafner J 1993 *Phys. Rev.* B **48** 13 115
Kresse G and Hafner J 1994 *Phys. Rev.* B **49** 14 251
[17] Kresse G and Furthmüller J 1996 *Comput. Mater. Sci.* **6** 15
Kresse G and Furthmüller J 1996 *Phys. Rev.* B **54** 11 196
[18] Hafner J and Kresse G 1997 *Properties of Complex Inorganic Solids* ed A Gonis, A Meike and P E A Turchi (New York: Plenum) p 69
[19] Vanderbilt D 1990 *Phys. Rev.* B **41** 7892
[20] Kresse G and Hafner J 1994 *J. Phys.: Condens. Matter* **6** 8245
[21] Furthmüller J, Kresse G and Hafner J 1994 *Phys. Rev.* B **50** 15 606
[22] Stadler R, Wolf W, Podloucky R, Kresse G, Furthmüller J and Hafner J 1996 *Phys. Rev.* B **54** 1729
[23] Moroni E G, Kresse G, Hafner J and Furthmüller J 1997 *Phys. Rev.* B **56** 15 629
[24] Langreth D C and Mehl M J 1983 *Phys. Rev.* B **28** 1809
[25] Perdew J P, Chevary J A, Vosko S H, Jackson K A, Pedersen M R, Singh D J and Fiolhais C 1992 *Phys. Rev.* B **46** 6671
[26] Becke A D 1992 *J. Chem. Phys.* **96** 2155
[27] Kresse G, Furthmüller J and Hafner J 1994 *Phys. Rev.* B **50** 13 181
[28] Seifert K, Hafner J, Furthmüller J and Kresse G 1995 *J. Phys.: Condens. Matter* **7** 3683
[29] Hamann D R 1996 *Phys. Rev. Lett.* **76** 660
[30] Allan D C and Teter M P 1987 *Phys. Rev. Lett.* **59** 1136
Allan D C and Teter M P 1990 *J. Am. Ceram. Soc.* **73** 3274
[31] Keskar N R and Chelikowsky J R 1992 *Phys. Rev.* B **46** 1
[32] Liu Feng, Garofalini S M, King-Smith R D and Vanderbilt D 1994 *Phys. Rev.* B **49** 12 528
[33] Teter D M, Gibbs G V, Boisen M B, Allan D C and Teter M P 1995 *Phys. Rev.* B **52** 8064
[34] Hamann D R 1995 *Phys. Rev.* B **51** 7337
[35] Liu Feng, Garofalini S H, King-Smith R D and Vanderbilt D 1993 *Phys. Rev. Lett.* **70** 2750
[36] Park K T, Terakura K and Matsui Y 1988 *Nature* **336** 670
[37] Cohen R E 1991 *Am. Mineral.* **76** 733
[38] Teter D M, Hemley R J, Kresse G and Hafner J 1998 *Phys. Rev. Lett.* **80** 2145
[39] Binggeli N, Chelikowsky J R and Wentzcovitch R M 1994 *Phys. Rev.* B **49** 9336
[40] Nada R, Catlow C R A, Dovesi R and Pisani C 1990 *Phys. Chem. Minerals* **17** 353
[41] Dovesi R, Pisani C, Roetti C and Silvi B 1987 *J. Chem. Phys.* **86** 6967
[42] Silvi B, d'Arco Ph and Causà M 1990 *J. Chem. Phys.* **93** 7225
[43] Silvi B, d'Arco Ph, Saunders V R and Dovesi R 1991 *Phys. Chem. Minerals* **17** 674
[44] Silvi B, Jolly L H and d'Arco Ph 1992 *J. Mol. Struct.* **260** 1
[45] Silvi B, Allavena M, Hannachi Y and d'Arco Ph 1992 *J. Am. Ceram. Soc.* **75** 1239
[46] Sherman D M 1993 *J. Geophys. Res.* **98** 11 865
[47] Holm J L, Kleppa O J and Westrum E F 1967 *Geochim. Cosmochim. Acta* **31** 2289
[48] Akaogi M and Navrotsky A 1984 *Phys. Earth Planet. Inter.* **36** 124
[49] Kihara K 1978 *Z. Kristallogr.* **148** 237
[50] Shropshire J, Keat P P and Vaughan P A 1959 *Z. Kristallogr., Kristallgeom., Kristallphys., Kristallchem.* **112** 409
[51] Smyth J R, Smith J V, Artioli G and Kvick A 1987 *J. Phys. Chem.* **91** 988
[52] Kohn W and Sham L J 1965 *Phys. Rev.* **140** A1133

[53] Mermin N D 1965 *Phys. Rev.* **140** A1141
[54] Perdew J P and Zunger A 1981 *Phys. Rev.* B **23** 5048
[55] Perdew J P 1986 *Phys. Rev.* B **33** 8800
[56] Becke A D 1988 *Phys. Rev.* A **38** 3038
[57] Wood D M and Zunger A 1985 *J. Phys. A: Math. Gen.* **18** 1343
[58] Pulay P 1980 *Chem. Phys. Lett.* **73** 393
[59] King-Smith R D, Payne M C and Lin J S 1991 *Phys. Rev.* B **44** 13 063
[60] Monkhorst H J and Pack J D 1976 *Phys. Rev.* B **13** 5188
Monkhorst H J and Pack J D 1978 *Phys. Rev.* B **18** 5897
[61] Jepsen O and Andersen O K 1991 *Solid State Commun.* **9** 1763
[62] Blöchl P, Jepsen O and Andersen O K 1994 *Phys. Rev.* B **49** 16 223
[63] Wallace D C 1972 *Thermodynamics of Crystals* (New York: Wiley) p 50
[64] Anderson O L 1995 *Equations of State of Solids for Geophysics and Ceramic Science* (Oxford: Oxford University Press)
[65] Dmitriev V, Torgashev V, Tolédano P and Salje E K H 1997 *Europhys. Lett.* **37** 553
[66] Dolino G 1990 *Phase Transitions* **21** 59
[67] Dove M T, Giddy A P and Heine V 1993 *Trans. Am. Crystallogr. Assoc.* **27** 65
[68] Tsuneyuki S, Aoki H and Tsukada M 1990 *Phys. Rev. Lett.* **64** 776
[69] Tezuka Y, Shin S and Ishigama M 1991 *Phys. Rev. Lett.* **66** 2356
[70] Angel R J, Allan D R, Miletich R and Finger F W 1997 *J. Appl. Crystallogr.* **30** 461
[71] Levien L, Prewitt C T and Weidner D J 1980 *Am. Mineral.* **65** 920
[72] Glinnemann J, King H E, Schulz H, Hahn Th, La Placa S J and Dacol F 1992 *Z. Kristallogr.* **198** 177
[73] Hazen R M, Finger L W, Hemley R J and Mao H K 1989 *Solid State Commun.* **72** 507
[74] Bass J D, Liebermann R C, Weidner D J and Finch S J 1981 *Phys. Earth Planet. Inter.* **25** 140
[75] Wright A F and Lehmann M S 1981 *J. Solid State Chem.* **36** 371
[76] *Landolt–Börnstein New Series* 1979 Group III, vol 11 (Berlin: Springer)
[77] Bruce A D and Cowley R A 1981 *Structural Phase Transitions* (London: Taylor and Francis)
[78] Grimm H and Dorner B 1975 *J. Phys. Chem. Solids* **36** 407
[79] Giddy A P, Dove M T, Pawley G S and Heine V 1993 *Acta Crystallogr.* A **49** 697
[80] Vallade M, Berge B and Dolino G 1992 *J. Physique* I **2** 1481
[81] Furthmüller J, Hafner J and Kresse G 1994 *Phys. Rev.* B **50** 15 506
[82] Wyckoff W L 1925 *Am. J. Sci.* **9** 448
Wyckoff W L 1925 *Z. Kristallogr.* **62** 189
[83] Barth T F W 1932 *Am. J. Sci.* **23** 350
[84] Nieuwenkamp W 1937 *Z. Kristallogr.* **96** 454
[85] Peacor D R 1973 *Z. Kristallogr.* **138** 274
[86] Wright A F and Leadbetter A J 1975 *Phil. Mag.* **31** 1391
[87] Barth T F W 1932 *Am. J. Sci.* **24** 97
[88] Nieuwenkamp W 1935 *Z. Kristallogr.* **92** 82
[89] Dollase W A 1965 *Z. Kristallogr.* **121** 369
[90] Pluth J J, Smith J V and Faber J 1985 *J. Appl. Phys.* **57** 1045
[91] Downs R T and Palmer D C 1994 *Am. Mineral.* **79** 9
[92] O'Keefe M and Hyde B G 1976 *Acta Crystallogr.* B **32** 2923
[93] Swainson I P and Dove M T 1993 *Phys. Rev. Lett.* **71** 193
[94] Kihara K 1980 *Z. Kristallogr.* **152** 95
Kihara K 1981 *Z. Kristallogr.* **157** 93
[95] Dollase W A 1967 *Acta Crystallogr.* **23** 617
[96] Kihara K 1977 *Z. Kristallogr.* **146** 185
[97] Dollase W A and Baur W H 1976 *Am. Mineral.* **61** 971
Baur W H 1977 *Acta Crystallogr.* B **33** 2615
[98] Kato K and Nukui A 1976 *Acta Crystallogr.* B **32** 2486
[99] Konnert J H and Appleman D E 1978 *Acta Crystallogr.* B **34** 391
[100] Geisinger K L, Spackmann M A and Gibbs G V 1987 *J. Phys. Chem.* **91** 3237
[101] Kirfe A, Will G and Arndt J 1979 *Z. Kristallogr.* **194** 315
[102] Levien L and Prewitt C T 1981 *Am. Mineral.* **66** 324
[103] Sugiyama M, Endo S and Koto K 1987 *Mineral. J. Japan* **13** 455
[104] Ross N L, Shu J F, Hazen R and Gasparik T 1990 *Am. Mineral.* **75** 739
[105] Juan Yu-min and Kaxiras E 1993 *Phys. Rev.* B **48** 14 994

[106] Jeanvoine Y, Kern G, Kresse G, Ángyán J G and Hafner J 1999 to be published
[107] Jeanvoine Y, Ángyán J G, Kresse G and Hafner J 1998 *J. Phys. Chem.* B **102** 5573
[108] Demuth Th and Hafner J 1999 to be published
[109] Liu L, Bassett W A and Takahashi T 1974 *J. Geophys. Res.* **79** 1160
[110] Jomard G, Petit T, Pasturel A, Kresse G and Hafner J 1999 *Phys. Rev.* B **59** 4044